



National  
Defence

Défense  
nationale



# TRANSIENT ANNEALING CHARACTERIZATION OF IRRADIATED MOSFETS (U)

by

T. Cousins and K.M. Qureshi

AD-A223 877

DTIC

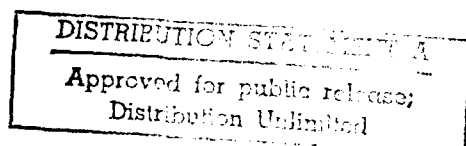
SELECTE

JUL 17 1990

D

DEFENCE RESEARCH ESTABLISHMENT OTTAWA  
REPORT NO.1030

Canada



January 1990  
Ottawa

90 07 16 307



National  
Defence

Défense  
nationale

# **TRANSIENT ANNEALING CHARACTERIZATION OF IRRADIATED MOSFETS (U)**

by

**T. Cousins and K.M. Qureshi**

*Nuclear Effects Section  
Electronics Division*

**DEFENCE RESEARCH ESTABLISHMENT OTTAWA**

**REPORT NO.1030**

PCN  
041LS

January 1990  
Ottawa

### ABSTRACT

The electrical response of metal-oxide-silicon (MOS) technologies to incident nuclear (especially photon) radiation is a very complex, time-dependent function. This report reviews the physical processes governing this response and then experimentally examines them with the aid of the TATS-400 (Transient Annealing Test System). MOSFET responses to steady-state and pulsed photon and electron beams are characterized in terms of such parameters as threshold voltage shift and interface and oxide trap densities. The results show good agreement between experiment and theory in terms of the expected trends, however in order to conduct more meaningful tests, devices with much better-known geometries must be procured.

### RÉSUMÉ

La réponse électrique des semiconducteurs de type MOS (métal-oxyde-silicium) aux radiations nucléaires est une fonction du temps très complexe. Ce rapport décrit les phénomènes physiques causant cette réponse et les étudie expérimentalement à l'aide d'un système de test TATS-400. La réponse de semiconducteurs de type MOSFET aux rayonnements continus et transitoires de photons et d'électrons démontre que les mesures s'accordent avec la théorie. Toutefois, des pièces dont les paramètres géométriques sont mieux connus sont nécessaires pour obtenir des résultats plus précis.



iii

Accession For	
NTIS GRA&I	<input checked="" type="checkbox"/>
DTIC TAB	<input type="checkbox"/>
Unannounced	<input type="checkbox"/>
Justification	
By _____	
Distribution/ _____	
Availability Codes	
Dist	Avail and/or Special
A-1	

## EXECUTIVE SUMMARY

The response of metal-oxide-silicon field-effect transistors (MOSFETs) to ionizing radiation (particularly gamma rays) is an extremely complex function of time, temperature, applied electric field and many other parameters. Prediction of the performance of electronic systems on the nuclear battlefield relies heavily, in many cases, on an understanding of this response. DREO has recently acquired the TATS 400 (Transient Annealing Test System) which allows fast current voltage curves of MOSFETs to be taken during and out to any time after irradiation. This report details the results of some preliminary tests using the TATS 400 with a variety of commercial MOSFETs subjected to nuclear weapon simulators. The results demonstrate conclusively that the annealing properties of MOSFETs may differ dramatically, but can be predicted if certain key manufacturing parameters are known. The TATS 400 shows great versatility as an experimental tool, and should prove extremely useful in future DREO work.

## TABLE OF CONTENTS

	<u>PAGE</u>
ABSTRACT/RÉSUMÉ . . . . .	iii
EXECUTIVE SUMMARY . . . . .	v
TABLE OF CONTENTS . . . . .	vii
LIST OF TABLES AND FIGURES . . . . .	ix
1.0 <u>INTRODUCTION</u> . . . . .	1
2.0 <u>THEORY</u> . . . . .	1
2.1 The Interaction of Radiation with MOSFETs . . . . .	1
2.2 Radiation Pulse Width Effects . . . . .	5
2.3 Charge Separation Techniques . . . . .	6
3.0 <u>EXPERIMENTAL</u> . . . . .	7
3.1 The TATS-400 System . . . . .	7
3.2 Steady-State Irradiation Experiments . . . . .	8
3.3 LINAC Irradiations . . . . .	9
3.4 Flash X-ray Irradiations . . . . .	10
4.0 <u>CONCLUSIONS</u> . . . . .	11
5.0 <u>REFERENCES</u> . . . . .	33

# LIST OF TABLES AND FIGURES

Page

## TABLES

TABLE 1	Categorization Matrix of MOS Device Response . . . . .	9
TABLE 2	Initial Threshold Voltage Shifts for Two Types of MOSFETS at APG FX Facility . . . . .	10

## FIGURES

Figure 1:	Schematic diagram of a simple (n-channel) MOSFET. Part (a) shows normal operation, while (b) refers to the postirradiation case . . . . .	13
Figure 2:	Energy band diagram of four major components of radiation response . . . . .	14
Figure 3:	Typical time dependence of $\Delta V_T$ following radiation pulse, showing the four major components discussed in the text . . . . .	15
Figure 4:	Predicted response of threshold voltage shift of MOSFET to radiation pulses of various widths. The generic impulse response from the text was used in the convolution here . . . . .	16
Figure 5:	Typical (idealized) set of I-V curves for MOSFET following pulsed irradiation . . . . .	17
Figure 6:	Schematic diagram of TATS . . . . .	18
Figure 7:	In-flux I-V curves for 3N171 MOSFET irradiated at DREO $^{60}\text{Co}$ GRM750 source. Total dose here was 55 kRad(Si) . . . . .	19
Figure 8:	Post-irradiation I-V curves for 3N171 MOSFET following irradiation as in fig (7). The annealing is followed from 10ms to 200,000s in a 1,2,5 time sequence . . . . .	19
Figure 9:	Plots of $\Delta V_T$ , $\Delta V_{OT}$ and $\Delta V_{IT}$ for the 3N171 both during and after steady-state irradiation. The parameters were derived using the techniques . . . . .	20

Figure 10: Comparison of the annealing characteristics of $\Delta V_{OT}$ of the 3N171 at $T = 25^\circ\text{C}$ and $T = 100^\circ\text{C}$ . The enhanced annealing at the higher temperatures is apparent . . . . .	21
Figure 11: In-flux characteristics of the 3N171 for steady-state irradiations at $25^\circ\text{C}$ and $100^\circ\text{C}$ . Note that more traps are filled at $25^\circ\text{C}$ , due to the higher temperature de-trapping . . . . .	22
Figure 12: I-V response curves of the 3N171 ( $V_g = 5\text{V}$ , $T = 100^\circ\text{C}$ ) following LINAC irradiation . . . . .	23
Figure 13: I-V response curves of the 3N171 ( $V_g = 20\text{V}$ , $T = 100^\circ\text{C}$ ) following LINAC irradiation . . . . .	23
Figure 14: Plot of $\Delta V_{OT}$ following LINAC irradiation for the two gate biases in fig (12) and fig (13). The accelerated annealing due to higher bias is readily apparent . . . . .	24
Figure 15: I-V response curves of the 2N12 ( $V_g = 5\text{V}$ , $T = 25^\circ\text{C}$ ) to LINAC irradiation . . . . .	25
Figure 16: I-V response curves of the 2N12 ( $V_g = 5\text{V}$ , $T = 100^\circ\text{C}$ ) to LINAC irradiation. Compare with Figure 15 . . . . .	25
Figure 17: I-V response curves of the 2N12 ( $V_g = 10\text{V}$ , $T = 25^\circ\text{C}$ ) to LINAC irradiation . . . . .	26
Figure 18: I-V response curves of the 2N12 ( $V_g = 10\text{V}$ , $T = 100^\circ\text{C}$ ) to LINAC irradiation. Compare with Figure 17 . . . . .	26
Figure 19: $\Delta V_{IT}$ characteristics of the 2N12 ( $V_g = 10\text{V}$ ) for two different temperatures following LINAC irradiation. Note the "stretchout" behaviour, and the effect of temperature . . . . .	27
Figure 20: I-V response curves for 2N12 ( $V_g = 10\text{V}$ , $T = 25^\circ\text{C}$ ) following Flash X-ray irradiation. Note the small shift due to smaller total dose, albeit higher dose rate than for the LINAC . . . . .	28
Figure 21: I-V response curves for 2N12 ( $V_g = 5\text{V}$ , $T = 100^\circ\text{C}$ ) following Flash X-ray irradiation. (Total dose $\sim 10 \text{ kRad}(\text{Si})$ ) . . . . .	28

Figure 22: I-V response curves for 2N12 ( $V_g = 10V$ , $T = 100^\circ C$ ) following Flash X-ray irradiation. (Total dose $\sim 10$ kRad(Si)). A comparison with fig 21 shows the effect of higher gate bias on "stretchout" . . . . .	29
Figure 23: I-V response curves for 3N171 ( $V_g = 10V$ , $T = 25^\circ C$ ) following Flash X-ray irradiation. (Total dose $\sim 10$ kRad) . . . . .	29
Figure 24: I-V response curve for 3N171 ( $V_g = 20V$ , $T = 100^\circ C$ ) following Flash X-ray irradiation. (Total dose $\sim 10$ kRad). The enhanced annealing compared to that in fig 23 is readily apparent . . . . .	30
Figure 25: I-V response curves for 2N12 ( $V_g = +10V$ , $T = 100^\circ C$ ), with bias switching as described in text, following Flash X-ray irradiation . . . . .	30
Figure 26: $\Delta V_{IT}$ behaviour of 2N12 for the switched bias test . . . . .	31
Figure 27: Comparison of annealing characteristics for switched bias and normal (+10V) conditions for 2N12 . . . . .	32



## 1.0 INTRODUCTION

The interaction of ionizing radiation with metal-oxide-silicon (MOS) technologies has, for the past quarter century, been the major focus of experimental and more importantly, theoretical studies on transient radiation effects on electronics (TREE). This is true not only because of the high susceptibility of MOS devices (particularly to gamma-ray irradiation) but because of the very well-defined geometries associated with modern MOS structures—allowing theoretical simulation. The problems associated with MOS devices will manifest themselves in bipolar technologies, as device dimensions shrink smaller and smaller. Thus the necessity of thoroughly understanding the interaction of radiation with MOS devices is an essential step toward the ultimate goal of all DREO TREE studies — the design/production /implementation of less radiation susceptible devices (and systems) into the CF.

As a first step toward an experimental examination of the interaction of photons with MOS devices, DREO recently purchased the TATS-400 (Transient Annealing Test System) (1). This system allows fast measurement of the I-V (current-voltage) characteristic curves of MOSFETs during, shortly after and for long times after either pulse or steady state irradiation. Thus, the various facets of the complicated time-dependent response may be observed. This report examines the theoretical response of MOS technologies to ionizing radiation, followed by some preliminary experiments with TATS which should serve to clarify these response characteristics.

## 2.0 THEORY

### 2.1 The Interaction of Radiation with MOSFETs

The following discussion follows very closely along the lines of an excellent review article by McLean (2). It concentrates exclusively on MOSFETs, although similar formulations can be applied to other MOS devices (such as capacitors).

Fig. 1 gives a schematic diagram of a simplified MOSFET. The channel here is of n-type. The theory of MOSFET transistor action is well known (3). Very simply, by applying a bias to the gate contact, an electric field is created in and immediately below the gate oxide. For sufficiently high (and in this case positive) potentials, majority carriers (holes in the p-type Si) are repelled from the surface region and, of course, minority carriers (electrons) are attracted — resulting in the creation of an "inversion layer". Now if a potential difference is applied across the source to drain contacts, this inversion layer will essentially act as a low-resistance channel for electron flow from source to drain. The turn on or threshold voltage ( $V_T$ ) is defined as that gate voltage at which the channel just begins to conduct current. Fig 1(a) illustrates these concepts.

Now, for the case of an irradiated MOSFET, the effect, in its broadest terms, is positive charge creation in the thin gate oxide region. This may be viewed as a radiation-induced gate voltage being created, and one obvious effect of radiation would then be a negative shift in  $V_T$ . In fact, for sufficiently large amounts of charge buildup, the MOSFET may be turned on (conducting current) even for  $V_g = 0$ . The device is then said to have failed by "going depletion mode". Fig 1(b) illustrates this case.

Although the preceding explanation of MOSFET-radiation response is sufficient to explain many gross effects, in order to better understand the physics of the radiation-induced interactions, it is necessary to consider the processes in much more detail.

Again following McLean, one may divide the radiation response of MOSFETs into four major components:

- (a) Electron/hole pairs generated by ionizing radiation;
- (b) 'Hopping' transport of holes through localized states in  $\text{SiO}_2$  bulk;
- (c) Deep hole trapping near  $\text{Si/SiO}_2$  interface; and
- (d) Radiation - induced interface traps within Si bandgap.

Each process is discussed in some detail below.

The generation of electron/hole pairs is, of course, the first process by which any ionizing radiation may interact with matter. In the first few picoseconds after irradiation, the free electrons may either recombine with the holes or be swept out of the oxide to be collected at the gate electrode. The holes, being much less mobile than electrons, remain during this time frame very near their point of generation. Thus an excess positive charge remains in the oxide and, as mentioned before, a negative voltage shift in  $V_T$  will occur. This initial (maximum) voltage shift ( $\Delta V_T(0^+)$  - where the  $0^+$  refers to the timeframe of a few picoseconds after irradiation) is determined by the initial hole yield multiplied by the fraction of holes which do not recombine. Experimentally this fraction has been measured and for  $^{60}\text{Co}$  and 12 MeV electrons is found to be of the order of 0.9 for gate oxide fields greater than  $\sim 1$  MeV/cm (4). Higher LET particles such as low energy x rays, protons and  $\alpha$  particles will generate a higher density of electron/hole pairs thus allowing more recombination and so the fraction is smaller.

Analytical expressions have been derived to predict this initial  $\Delta V_T(0^+)$ . The two major governing factors are the radiation dose and oxide thickness. (The fact that the oxide thickness is a major factor is of course the basis for many rad-hard, thin oxide technologies). From experiments, the electron/hole pair creation density per unit dose is  $g_0 = 8.1 \times 10^{12} \text{ cm}^{-3} \text{ rad}^{-1} (\text{SiO}_2)$  (4). One may use this in an expression for the initial threshold voltage shift as:

$$\Delta V_T(0^+) = [q g_0 d_{ox} f_V(E_{ox}) D] / 2 C_{ox} \quad (1)$$

where

$q$  = electron charge

$d_{ox}$  = oxide thickness

$f_y (E_{ox})$  = fractional hole yield after recombination

$E_{ox}$  = electric field across the oxide

$D$  = radiation dose

and  $C_{ox} = \epsilon_{ox}/d_{ox}$

Substituting

$$\Delta V_T (0^+) = 1.9 \times 10^{-8} d_{ox}^2 f_y (E_{ox}) D \quad (2)$$

Now  $\Delta V_T (0^+)$  is in volts if  $d_{ox}$  is in nanometres and  $D$  is in Rads ( $\text{SiO}_2$ ). This equation is very useful not only for predicting voltage shifts if  $d_{ox}$  is known, but provides a way to measure  $d_{ox}$  - a parameter which is not always readily available from the manufacturer.

Following the hole generation a second process occurs as the holes drift due to the electric field toward the Si/SiO<sub>2</sub> interface. This process is stochastic in nature and may last from 10<sup>-7</sup> s to many s - giving rise to short-term transient recovery in the original negative voltage shift. The movement of holes through the oxide has been attributed to a 'hopping' process from one site to another with the possibility of discrete trapping events occurring at some of these sites which last for time periods longer than the oxide transit time of the fastest carriers. Thus the wide dispersion in transit times results. An energy band diagram of the hopping transport phenomenology and the three other components of MOS response is given in Fig. (2).

A continuous-time-random-walk (CTRW) formulism (eg (5) (6) (7)) has been developed to successfully explain hole transport in SiO<sub>2</sub>. From this, an expression for  $t_s$  - the time for half recovery of the threshold voltage shift has been developed as:

$$t_s = t_s^0 (d_{ox}/a)^{1/\alpha} \exp [\Delta E_{ox}/k_B T] \quad (3)$$

where

$t_s^0$  is a constant

$a$  = hopping distance

$k_B$  = Boltzmann Constant

$T$  = temperature

One may use for many (hardened) oxides  $\alpha = 0.25$ . Note the large effects of temperature and applied field and thickness on recovery time. Thus for a 0.5  $\mu\text{m}$  vs 50 nm device, there is a 10<sup>4</sup> difference in recovery time.

Following the hole transport to the Si/SiO<sub>2</sub> interface, a certain percentage of the holes may be trapped within ~ 10 nm of the interface. This trapping is very-long lived and may last from hours to years - producing a

remnant negative voltage shift. This shift is the most commonly observed in MOSFET irradiations - and is the basis for the new CF dosimeter (8).

The physical origin of the trapping process is believed to be a deficiency of oxygen atoms at the Si/SiO<sub>2</sub> interface which results in a large number of strained Si-Si bonds (instead of the normal Si-O-Si configuration). A hole entering such a strained bond may break it and recombine with one of the bonding electrons. The resulting positively charged structure relaxes to the E<sub>1</sub> centre configuration, with one of the Si atoms retaining the remaining electron from the broken bond, whilst the other accepts the positive charge.

The discharge of these hole traps (often referred to as long-term annealing) is observed to follow a tunnel annealing formalism with the V<sub>T</sub> recovery being roughly linear with log (time). The model to explain this (9,10) assumes that electrons from the substrate tunnel to, and recombine with the trapped holes near the interface. At any time t, the hole traps are emptying at a depth X<sub>m</sub>(t) (from the Si) that increases logarithmically with time, i.e.

$$X_m(t) = (1/2\beta) \ln (t/t_0) \quad (4)$$

where

$\beta$  = tunnelling barrier height parameter  
t<sub>0</sub> = time scale parameter

This implies the movement of a "tunnelling front" with velocity  $\Delta X_m = 1.15/\beta$  per decade in time. Experimentally  $\Delta X_m$  has been found to be roughly 0.2 nm per decade (11). Other experiments have shown that the true  $\Delta V_T(t)$  distribution is not completely exponential but flattens out with time. An exponential falloff of trapped hole density can explain this (12). These models (12) can also show that hardened structures have a much sharper trapped hole density drop off with distance from the interface than their softer counterparts. So one would expect much slower annealing from the softer devices.

(Note that hardened devices are those which have been purposely manufactured so that the initial threshold voltage shift will be smaller, and/or the annealing process will be faster than for normal (softer) devices. Techniques designed to harden include thinner oxides and a sharper interface).

The final process in MOSFET response is due to radiation-induced traps. These are localized electronic states near the interface, which have energy levels distributed within the Si bandgap. These traps may either be prompt in nature (i.e. created by a LINAC pulse) or time-dependent-building up for thousands of seconds. The main effects of these traps are to produce (non-linear) distortions (such as stretchout) in the I-V characteristics, shift V<sub>T</sub> and introduce additional scattering centres.

The time dependence of the four processes is shown in Fig. (3). Note that, in this figure, at long times, and if the interface trap buildup is

large enough 'super recovery' or 'rebound' may occur, where the value of  $V_T$  actually becomes positive.

## 2.2 Radiation Pulse Width Effects

As mentioned in a previous DREO report (13) the highly time-dependent response function of MOS devices will lead in general to different observed device responses depending on the width (as well as intensity) of the initial radiation pulse. Since, for battlefield purposes, we generally think of only steady-state (fallout) or extremely fast (initial pulse) scenarios, there is a tendency to lump the MOSFET response to a pulse under the dose-rate effects category. This is however inappropriate since dose-rate effects invariably imply photocurrent generation. The term 'pulse-width dependent total dose effects' is more appropriate when discussing MOS response.

The response of a MOSFET to an arbitrary pulse shape  $S(t')$  is simply the convolution of  $S(t')$  with the impulse response function  $R(t-t')$ , i.e.

$$\Delta V_T(t) = \int_0^t S(t') R(t-t') dt' \quad (5)$$

Fig. (4) illustrates the differences which would be observed in  $\Delta V_T(t)$  dependent upon some specific widths  $S(t')$ .

For these calculations, a generic impulse response function ( $R(t-t')$ ) was assumed, as given by McLean (14)

$$R(t) = \Delta V_\infty + (\Delta V_0 - \Delta V_\infty)/(1 + t/\tau_0)^\nu \quad (6)$$

where

- $\Delta V_\infty$  = impulse response function at  $t = \infty$
- $\Delta V_0$  = impulse response function at  $t = 0$
- $\tau_0$  = characteristic time for device response (i.e. characteristic trapping time)
- $\nu$  = experimentally determined constant.

The input pulses here represent square waves of 10 ns, 1  $\mu$ s and 1 ms duration. The pulse heights, and hence the dose rates were all the same.

The assumptions made on the response were that  $V_\infty = 0$  and  $V_0 = 1$ , with  $\nu = 0.25$  which is typical from experimental data (14). A characteristic time,  $\tau_0$ , of  $10^{-5}$ s was assumed - i.e. fast trapping processes dominate.

The very differing shapes immediately following pulse cessation are due to the ratio of pulse width time ( $\tau_w$ ) to trapping time. Note that only for the two shortest pulse widths can the effects of the trapping (flat portion of the curve) be readily observed. This emphasizes a rough rule of thumb - in order to observe a (trapping) phenomenon with time constant  $\tau_0$ , the pulse

width  $\tau_w$  should be  $\tau_w \leq \tau_0$ . This has been shown for impurity charge trapping in GaAs devices (13).

Thus to accurately simulate battlefield performance, an accurate pulse shape simulator must be used. However to study basic physical mechanisms a wide range of pulse widths is absolutely necessary.

### 2.3 Charge Separation Techniques

Assuming that enough time has elapsed after irradiation to allow hole transport to have finished, then the threshold voltage shift is just

$$\Delta V_T = \Delta V_{ot} + \Delta V_{it} \quad (7)$$

where  $\Delta V_{ot}$  and  $\Delta V_{it}$  are the voltage changes due to oxide and interface trapped charges respectively.

In order to perform complete experimental testing, it is necessary to know the relative magnitudes of each component and so a methodology has been devised to separate the two. The primary technique used by most (2) makes the assumption of net charge neutrality of  $\Delta N_{it}$  (the density of interface traps) at the midgap voltage - i.e. the value of applied bias is such that the Fermi level at the Si/SiO<sub>2</sub> interface is at the midpoint of the Si bandgap. By definition the oxide trapped charge does not change its occupancy or charge state as the bias varies. Therefore, with the assumption of midgap neutrality of  $\Delta N_{it}$ , the radiation induced voltage shift ( $\Delta V_{mg}$ ) of the subthreshold MOSFET device characteristics can be attributed solely to the oxide trapped charge

$$\Delta V_{mg} = q \Delta N_{ot} / C_{ox} = \Delta V_{ot} \quad (8)$$

Thus, from two measurements  $\Delta V_{mg}$  and  $\Delta V_T$  charge separation is accomplished, i.e.

$$\Delta V_{it} = q \Delta N_{it} / C_{ox} = \Delta V_T - \Delta V_{mg} \quad (9)$$

A rigorous experimental determination of  $\Delta V_{mg}$  and  $\Delta V_T$  is not trivial, and for most commercial devices the parameters required to calculate them are not available. A typical set of post-pulse annealing I-V curves for a MOSFET are shown in Fig. (5). In order to determine a  $V_{mg}$  and  $V_T$ , normally the associated currents are calculated, and for each curve, the corresponding voltages are determined from these curves. An example of the complexity associated with these current calculations can be garnered from Sze (15). The threshold current may be written:

$$I_{th} = \mu_n (Z/L) a C_i / 2 \beta^2 (n_i / N_A)^2 (1 - e^{-\beta V_0}) e^{\beta \chi_s} (\beta \chi_s)^{-1/2} \quad (10)$$

All of the terms will not be explained but some, such as  $a$  (dependent on oxide thickness),  $L$  (dependent on channel length),  $n_i$  (dependent on doping parameters) and  $C_i$  (dependent upon capacitance) are manufacturer determined and their exact values not normally available.

Fortunately, McWhorter and Winokur (16) have shown that the exact values of  $I_t$  and  $I_{mg}$  are not extremely critical to determining  $\Delta V_{it}$  and  $\Delta V_{ot}$ . Indeed a factor of 10 variation in either may have only ~ 10% change in the trap concentration determinations. As a very good approximation, one may use  $I_{th} = 10^{-6}$  A and  $I_{mg} = 10^{-13}$  A (17) over the entire range. The values of  $V_{th}$  and  $V_{mg}$  may then be read directly for each I - V curve. (One should note that the value of  $10^{-13}$ A is too small to be directly read from the I-V curves, and so extrapolation must be used (16)).

The McWhorter formulism for deriving the trap densities follows directly. The definition of a "stretchout" voltage  $V_{so}$  as

$$V_{so} = V_{th} - V_{mg} \quad (11)$$

allows simply

$$\Delta V_{it} = (V_{so})_2 - (V_{so})_1 \quad (12)$$

and as before (7)

$$\Delta V_{ot} = (V_{mg})_2 - (V_{mg})_1 \quad (13)$$

Here the subscripts 1 and 2 refer to consecutive (in-time) I-V curves.

### 3.0 EXPERIMENTAL

#### 3.1 The TATS-400 system

The TATS-400 system is shown schematically in Fig. 6. The TATS unit contains the electronic circuitry which performs all the detailed timing, parts biasing and current measurements and temporarily stores the measured readings. Each measurement card associated with TATS is an independent, microprocessor controlled test system which can communicate with the PC, measure elapsed time from test start and program drain, source, substrate and gate voltages. At appropriate times, each card will force a series of source currents and measure the associated gate voltage. Thus a series of I - V curves is obtained as a function of time (which may be during irradiation (and thus correspond to dose) or after irradiation (and thus simply annealing)).

A temperature control subsystem allows testing over the full military range ( $-55^{\circ}\text{C}$  to  $+125^{\circ}\text{C}$ ). Typically, measurements can be made from ~ lms after (pulse) irradiation out to an effectively infinite time.

### 3.2 Steady-State Irradiation Experiments

The steady-state irradiation of MOSFETs experiments took place at the GRM750  $^{60}\text{Co}$  gamma-ray source at DREO. The device chosen for these irradiation was the Motorola 3N171 n channel MOSFET. Figs 7 and 8 respectively show the in-flux and post-irradiation I-V curves as taken by TATS for one of these experiments. Here, both irradiation and annealing measurements were made with a gate voltage of +5V, and at a temperature of +25°C. The total dose delivered was 55 kRad(Si) over 20,000 s (5.56h). The annealing was followed up to 200,000 s (55.6h) after irradiation. Both sets of curves are in a 1,2,5 time sequence starting at 10 ms.

Following along the lines presented in the analysis section, Fig 9 shows plots for  $\Delta V_T$ ,  $\Delta V_{OT}$  and  $\Delta V_{IT}$  for the 3N171 both during irradiation and annealing. Clearly for this device the contribution of oxide traps during irradiation greatly exceeds that from the interface, and the annealing is also dominated by the oxide traps. Boesch (18) has proposed a classification scheme to categorize MOS response, shown in table (1). The 3N171 would apparently fall into category 2.

The effect of temperature on the irradiation and annealing trap behaviour was then investigated. Fig 10 shows the  $\Delta V_{OT}$  characteristics for anneals at temperatures of 25°C and 100°C, both following a 55 kRad (Si) irradiation at 25°C. The curves have been normalized to each other at  $t = 100\text{s}$ . The accelerated de-trapping due to temperature is readily apparent. Both exhibit a  $\log(t)$  behaviour, with characteristics recovery times (to reach 1/2 of  $(\Delta V_T(o^+) - \Delta V_T(50,000\text{ s}))$ ) of 10,000 s for the 25°C case and 1000 s for the 100°C case.

The effect of temperature on the I-V characteristics during irradiation is shown in fig 11. Note that the net number of traps created at 25°C exceeds that at 100°C (for the same doses) due to the enhanced annealing effects discussed above - which occur simultaneously with the trap creation.



**TABLE 1**

Categorization Matrix of MOS Device Response  
( $\Delta N_{ot}$  refers to trapped hole density before annealing occurs)

	$\Delta N_{it} \ll \Delta N_{ot}$	$\Delta N_{it} \approx \Delta N_{ot}$
	<u>Category 1</u>	<u>Category 3</u>
Low $\Delta N_{ot}$	No Superrecovery Moderate $\log(t)$ recovery Negligible mobility Degradation Hard	Some Superrecovery Complex time History Some Mobility Degradation Hard
	<u>Category 2</u>	<u>Category 4</u>
High $\Delta N_{ot}$	No Superrecovery Weak $\log(t)$ recovery Possible mobility Degradation Soft	Large Superrecovery Complex time history Severe Mobility Degradation Soft

### 3.3 LINAC Irradiations

Irradiations with an electron linear accelerator (LINAC) were carried out at the MEVEX (19) facility, Stittsville, Ontario. The machine, normally capable of producing a train of  $2\mu s$  pulses was modified for this work so as to be swept, when triggered, to produce one single  $2\mu s$  pulse at the device being irradiated. No shot-to-shot dosimetry was directly carried out for this work, however a nominal total dose of 22 kRad(Si) ( $\dot{\gamma} \approx 1 \times 10^{10}$  Rad(Si)/s) was inferred from separate dosimetry measurements.

Figs 12 and 13 show the I-V response curves to the LINAC pulse for the 3N171 devices at 100°C for gate voltages of +5 and +20V respectively. Note the enhanced annealing at the higher gate voltage, which is also shown in fig 14 from the  $\Delta V_{ot}$  portion of the curve. The parallel nature of the I-V curves and rough  $\log(t)$  recovery again place this device in category 2.

Figs 15-18 shown the response to the LINAC pulse of an RCA RFP 2N12 n-channel MOSFET, for various gate voltages and temperatures. While the expected trends are readily apparent, the nature of this device response is noticeably different from the 3N171. The initial post-irradiation I-V curve for the 2N12 is simply shifted along the negative voltage axis, and roughly parallel to the pre-rad curve - a clear indication of positive charge being induced in the oxide. This parallel behaviour is maintained for the first few post-irradiation sweeps. However for the later sweeps the I-V curves exhibit a strong "stretchout" behaviour, with the contribution from  $\Delta N_{it}$  (the delayed build up of interface traps) becoming dominant. Fig 19 shows this effect more

dramatically. The complex time history of  $V_T$  for the 2N12 would suggest a category 4 classification for this device.

### 3.4 Flash X-Ray Irradiations

As a complement to the LINAC work, irradiations were also carried out using the Physics International Flash X-ray machine located at the Nuclear Effects Directorate, Aberdeen Proving Ground, U.S. (20). This machine produces a nominal 80 ns wide pulse of 4 MeV Bremsstrahlung photons. For this work  $\text{CaF}_2\text{:Mn}$  TLDs were positioned as close as possible to the device under irradiation in order to ascertain the dose delivered for each shot.

Fig 20 shows the I-V curves for a 2N12 device again spanning time from 10 ms to 1000 s after irradiation. The transistor was at room temperature, with a gate bias of +10V. Note the very small shift here. The total measured dose here was 3295 Rads(Si) or a dose rate of  $4.1 \times 10^{10}$  Rads(Si)/s, which is a considerably greater dose rate than experienced at the LINAC. However, again, the effect is not dose-rate dependent, but rather total dose-pulse width dependent, and the total dose is almost an order of magnitude less than experienced at the LINAC.

With the shot-by-shot dosimetry it was possible to check the validity of eq'n (2) for initial threshold voltage shift. This is done in table (2).

TABLE 2

Initial Threshold Voltage Shifts for Two Types of  
MOSFETs at APG FX Facility

3N171		
TLD#	D <sub>γ</sub> (Rad(Si))	ΔV <sub>T</sub> (0 <sup>+</sup> )
17	12956	-3.79
21	14132	-4.10
30	7705	-3.78
2N12		
TLD#	D <sub>γ</sub> (Rad(Si))	ΔV <sub>T</sub> (0 <sup>+</sup> )
47	8569	-1.24
32	9469	-1.69
32	9469	-1.19
44	10360	-1.22
44	10360	-1.40

The evaluated gate oxide thicknesses from this table are  $d_{ox} = (144 \pm 46)$  nm for the 3N171 and  $d_{ox} = (90 \pm 15)$  nm for the 2N12. The latter value is somewhat greater than the manufacturer's quoted value of  $d_{ox} = 55$  nm, even with the lower error bound. Two explanations are possible here; either eq'n (2) may be used only as a rough guideline (i.e. the 3N171 has a thicker oxide than the 2N12) or the information available from the manufacturer is not adequate enough. The latter reason can only be abrogated by strict, DREO-controlled manufacturing techniques.

Figs 21 - 24 show the pulse response of the 2N12 and 3N171 for a variety of temperature and gate bias settings. The same trends (and thus same categorizations) are apparent as for the LINAC work.

Fig 25 shows the I-V response curve for a 2N12 device under different biasing conditions. Here the gate bias was held at -10 V before, during and for 500 s after irradiation then switched to +10V for the next 500 s. Annealing was followed for the entire time period (at 100°C).

The behaviour of the interface traps here is quite interesting as shown in fig 26. Very little annealing occurs during the negative gate bias portion of the curve, while immediately upon the switch to the positive bias a large anneal occurs in the first one second, followed by a very slow anneal for the next 500 s. Fig 27 shows a comparison of the annealing (at +10V, 100°C) characteristics for the 2N12 both with and without the negative bias cycle. The trend here would seem to indicate an enhanced early (<1s) annealing for the switched bias case, followed by a decrease in the annealing rate for later (≥100s) times. This may be evidence for some tunneling during the negative bias stage, resulting in an enhanced buildup of holes near the interface which may then move more quickly than for the normal case. Lelis et al (21) have done substantial work on the bias-dependence of annealing and attribute the phenomenology to electrons tunneling back and forth from the Si substrate to electron traps in the oxide. The 2N12 would appear to be a candidate for future more detailed bias-switching work.

#### 4.0 CONCLUSIONS

The TATS-400 system has proven itself a versatile and useful tool for examination of the response of MOS devices to photon irradiation, both steady-state and pulse. The system is capable of performing both pure physics studies (such as the phases and causes of annealing) and applied research (such as the performance of the new CF MOSFET dosimeter). The temperature and biasing variability are essential for accurate studies, and will be invaluable in future research.

This work has also shown some inadequacies in the current DREO TREE capabilities which must be remedied in order to establish a fully viable program. Firstly it is essential the DREO have its own on-site LINAC facility, specifically tailored to produce the wide variety of pulse widths (ns to μs) necessary for complete annealing studies. (As an aside, these pulse widths are essential for other studies such as electron trap-depth in GaAs, etc.). To test completely any one device requires a great many (perhaps 10-20) biasing/temperature/dose scenarios. Thus it is essential that DREO have full-time and continuous access to its own dedicated LINAC facility.

Secondly, in order to understand fully the basic interactions at the microscopic scale, it is imperative that DREO have access to a device design and fabrication facility. All parameters (gate oxide thickness, width, etc.) must be known exactly prior to any meaningful work. This is especially true for theoretical studies. These parameters are not generally available from the manufacturers, and so well-characterized experiments cannot be carried out with commercial products.

Even with these inadequacies, this work has shown that there are dramatic differences in various MOSFET response to (photon) irradiation. This implies that the TATS-400 system may be used for test and evaluation of prototype and commercial transistors (and other MOS technologies) to determine their response on the battlefield and thus determine the efficacy of CF electronic systems.

It is expected that the TATS 400 will be a prime force in future MOS experimental work by DREO, both in-house and collaborative.

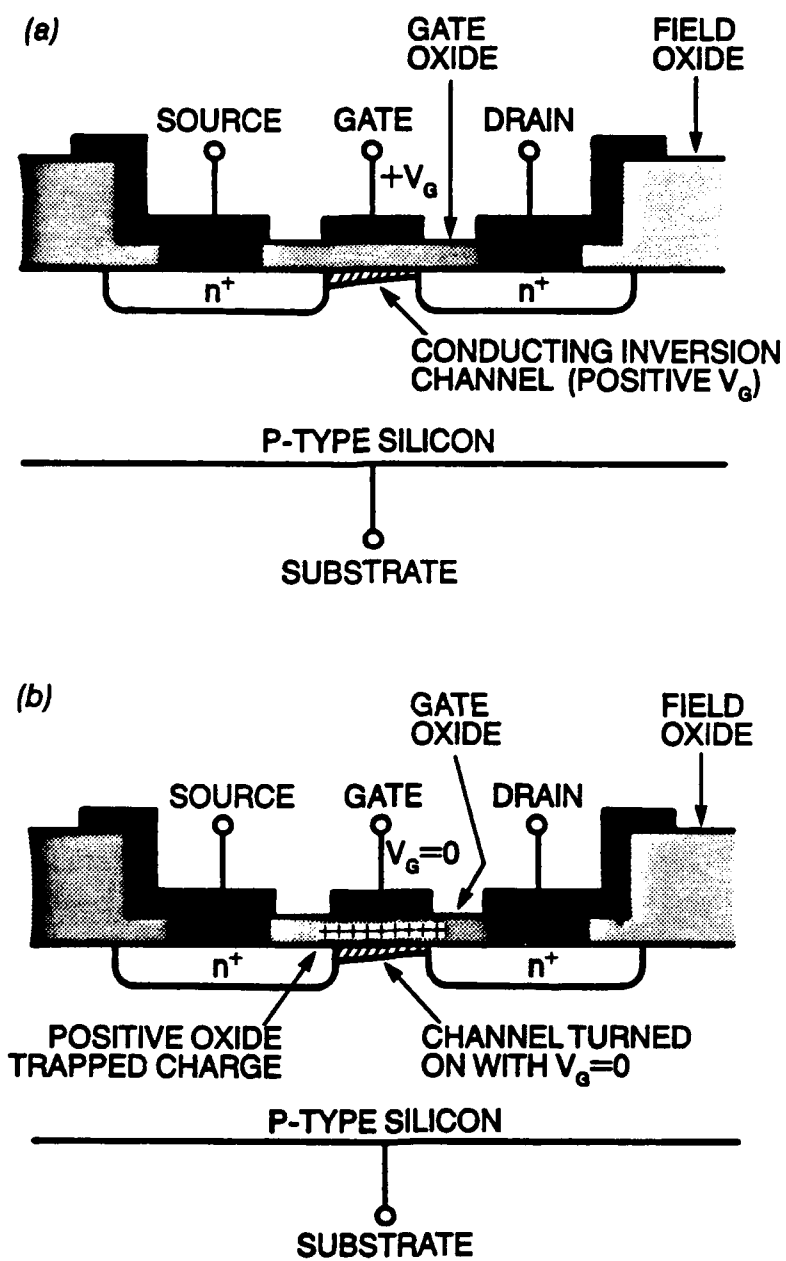


Figure 1: Schematic diagram of a simple (n-channel) MOSFET. Part (a) shows normal operation, while (b) refers to the postirradiation case.

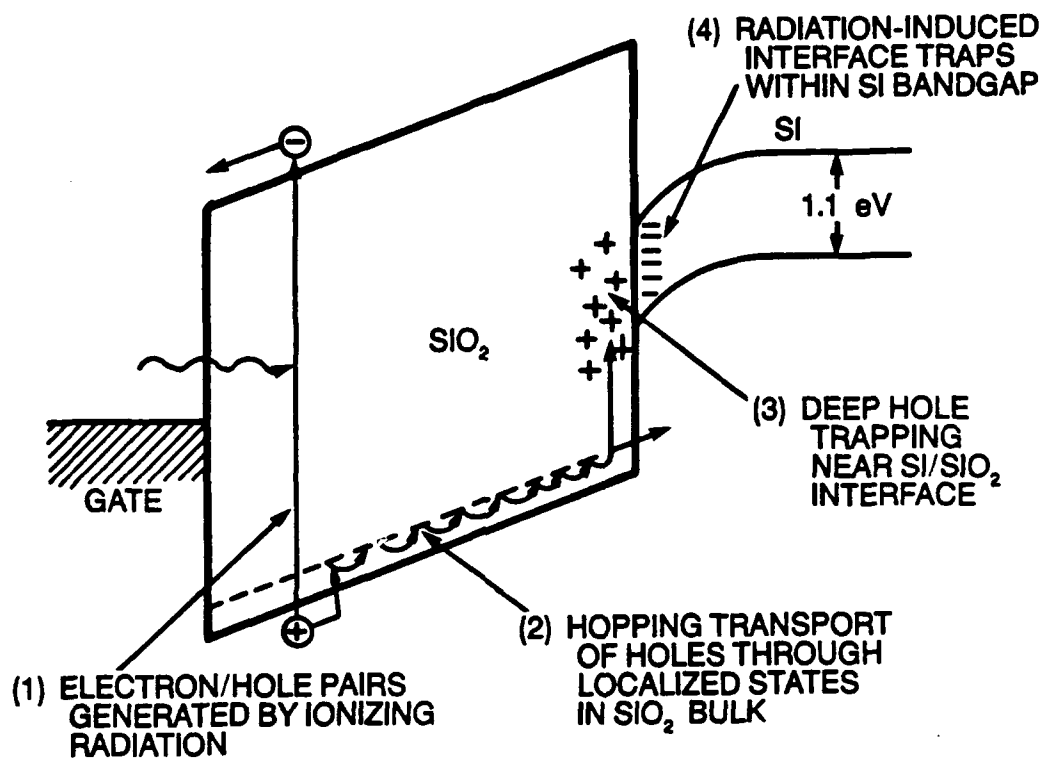


Figure 2: Energy band diagram of four major components of radiation response.

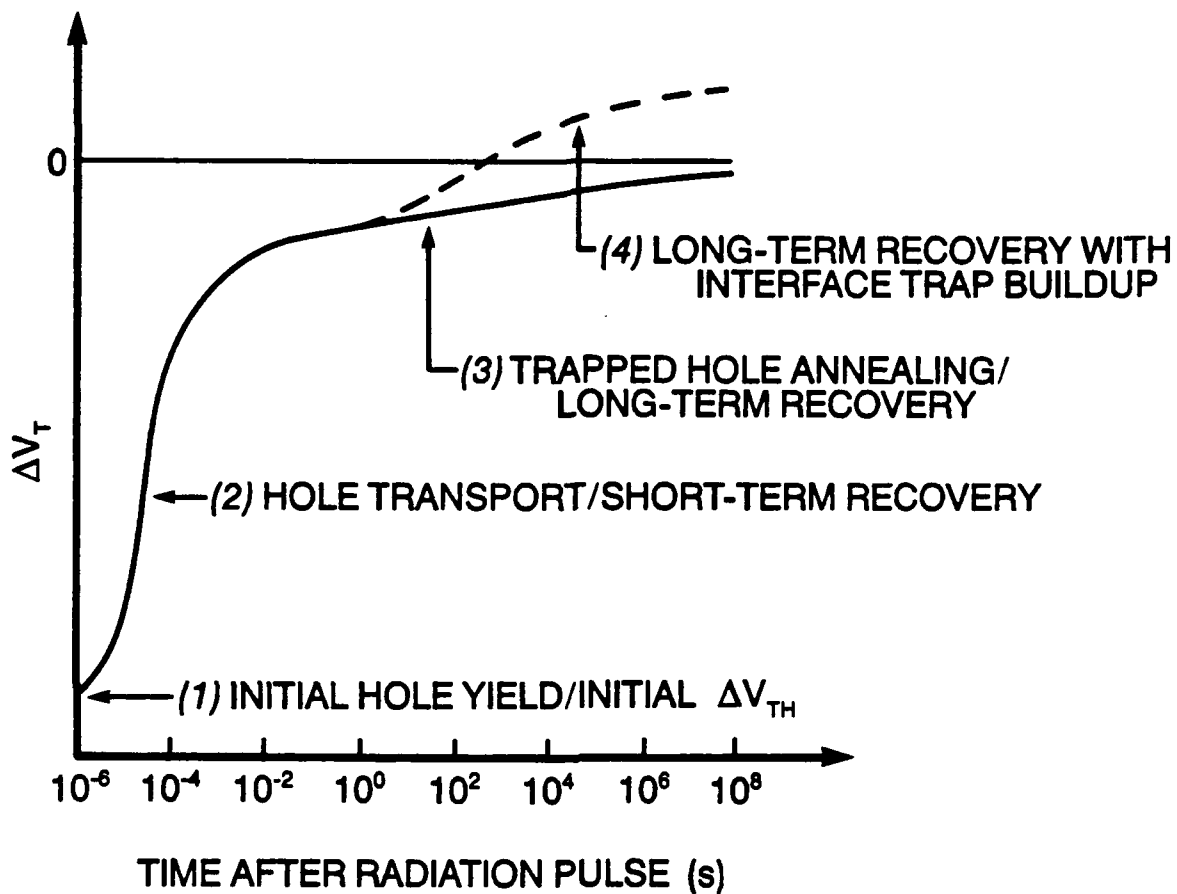


Figure 3: Typical time dependence of  $\Delta V_T$  following radiation pulse, showing the four major components discussed in the text.

# MOS GENERIC RESPONSE 3 PULSE WIDTHS

de l t a v t - a r b i t r a r y u n i t s

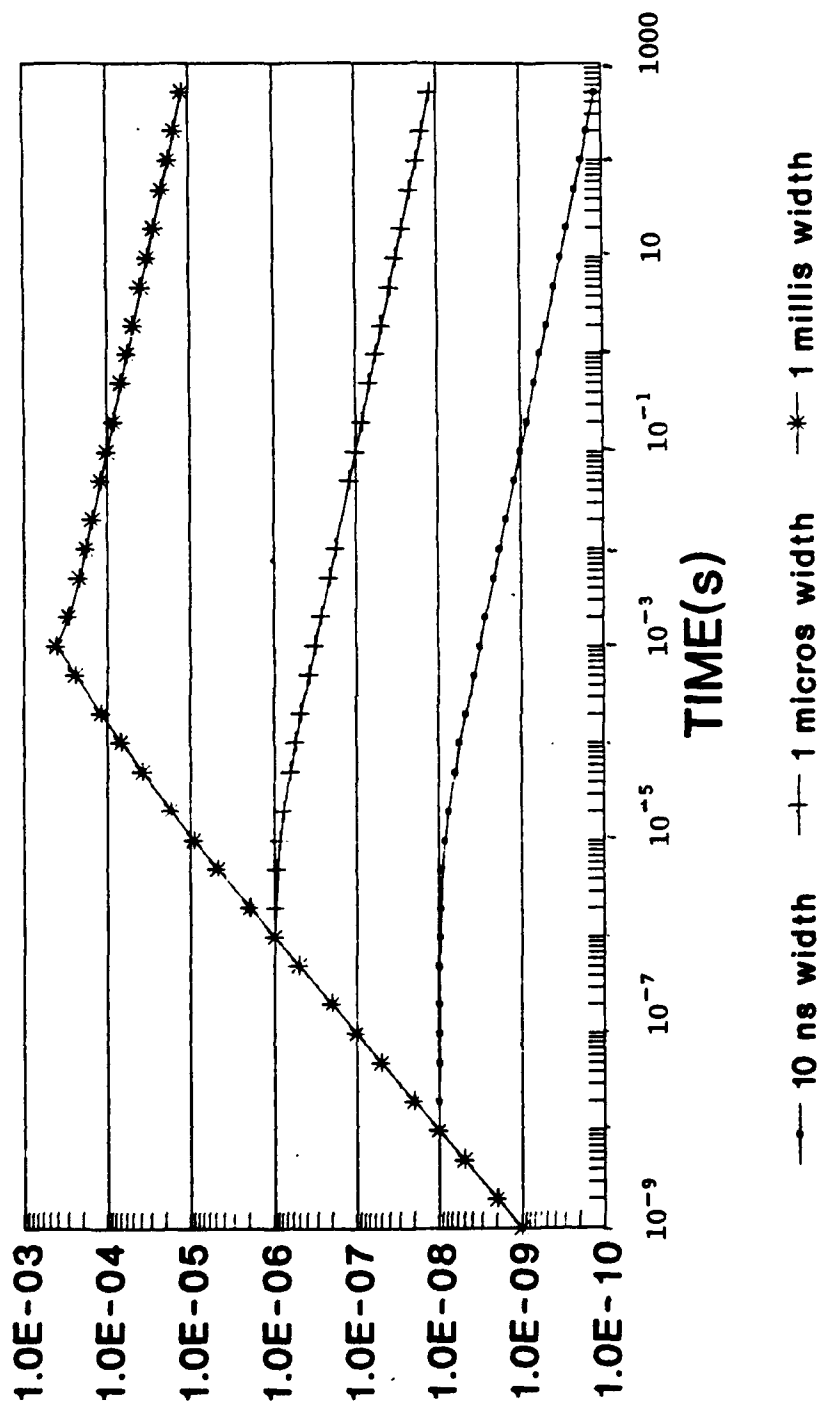


Figure 4: Predicted response of threshold voltage shift of MOSFET to radiation pulses of various widths. The generic impulse response from the text was used in the convolution here.



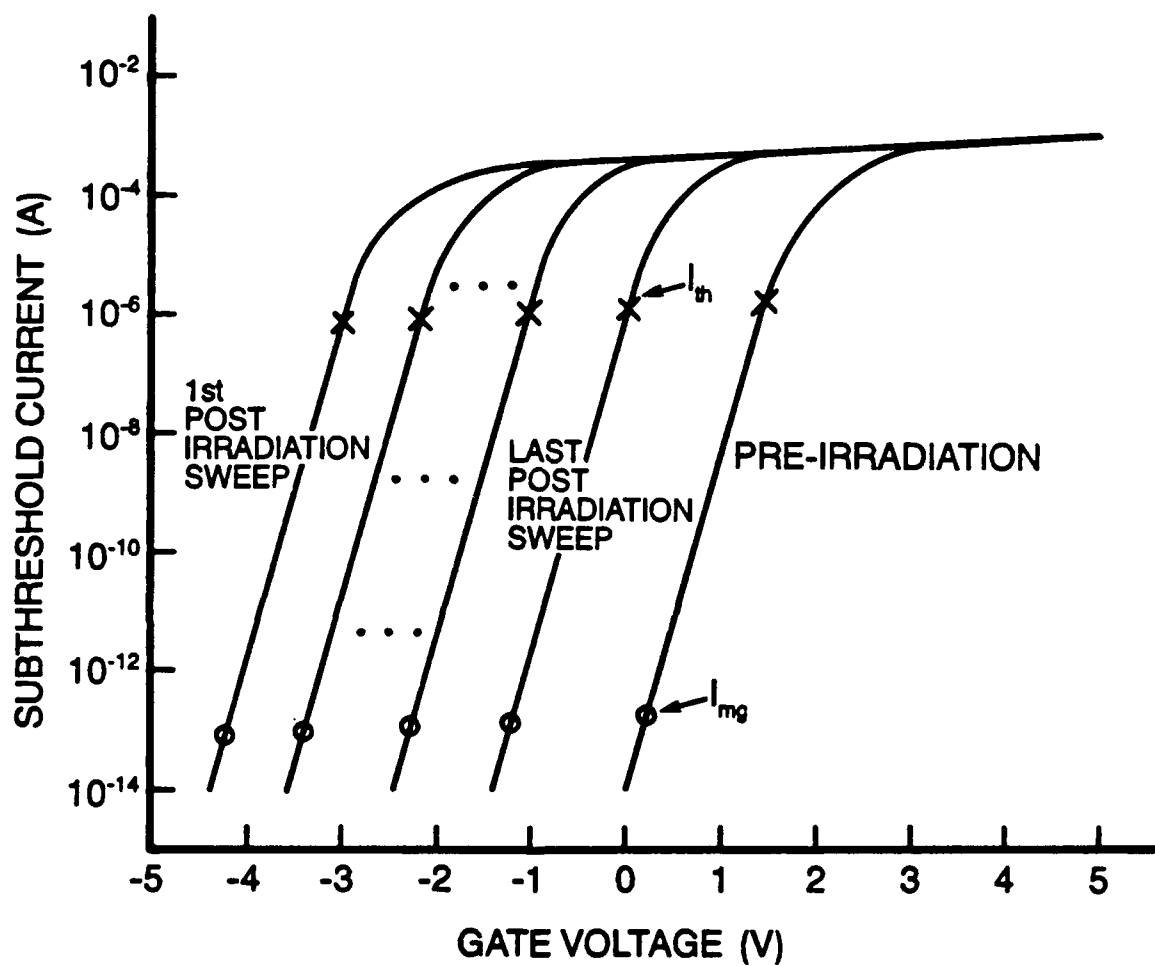


Figure 5: Typical (idealized) set of I-V curves for MOSFET following pulsed irradiation.

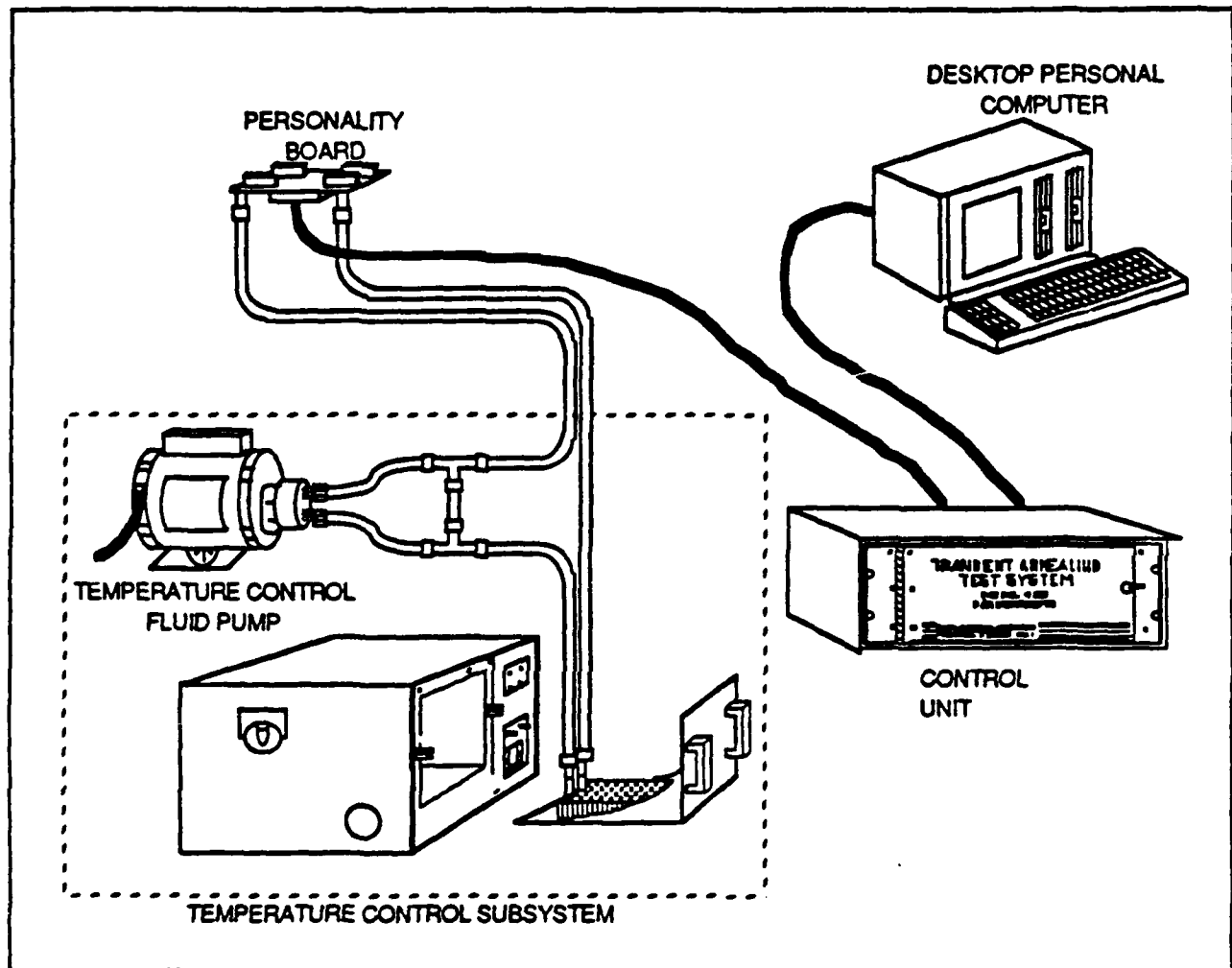


Figure 6: Schematic diagram of TATS.

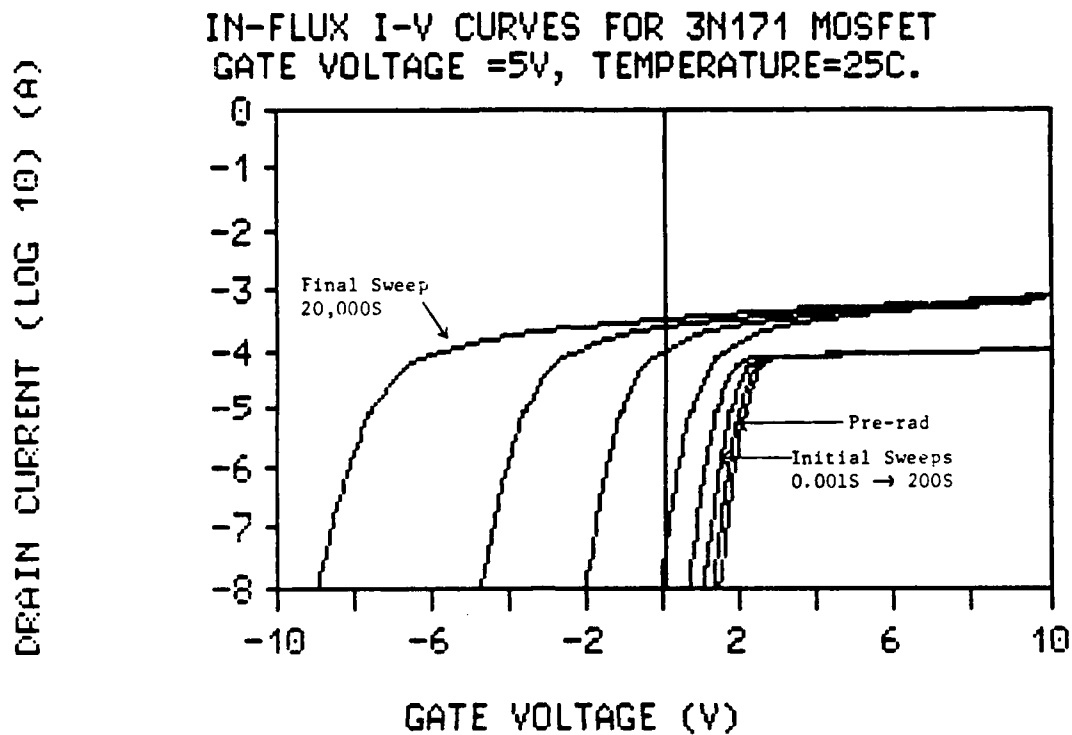


Figure 7: In-flux I-V curves for 3N171 MOSFET irradiated at DREO  $^{60}\text{Co}$  GRM750 source. Total dose here was 55 kRad(Si).

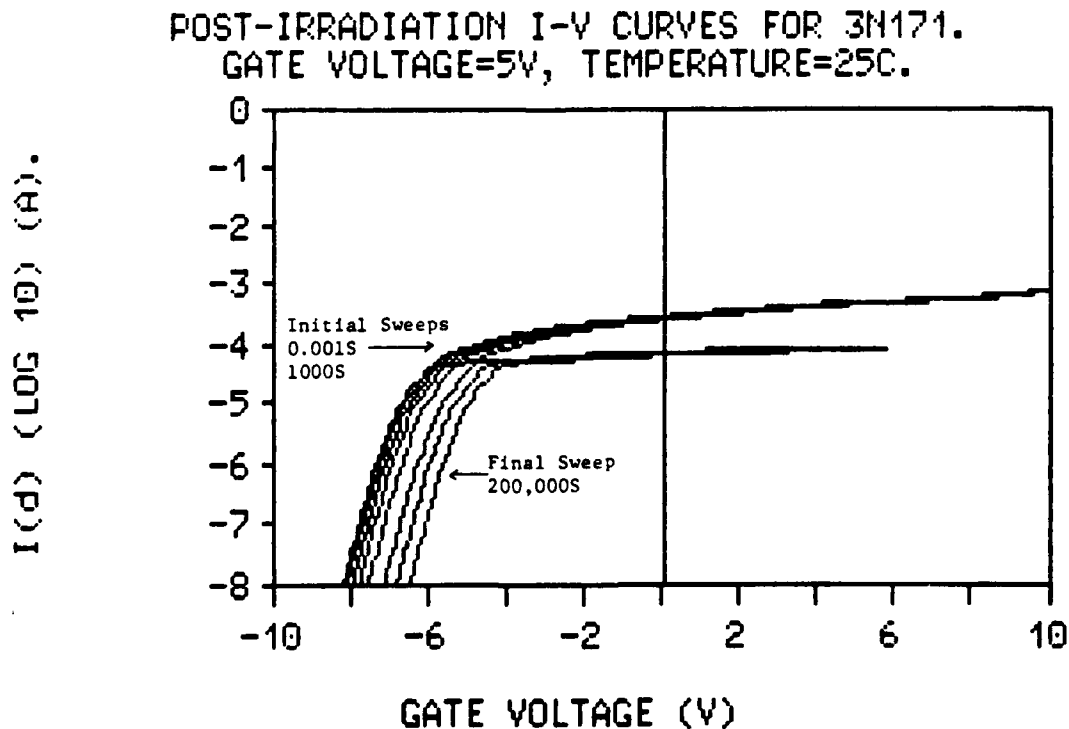


Figure 8: Post-irradiation I-V curves for 3N171 MOSFET following irradiation as in fig (7). The annealing is followed from 10ms to 200,000s in a 1,2,5 time sequence.

# PLOT OF $V_{thres}$ , $V_{ot}$ and $V_{it}$ BOTH DURING IRRADIATION AND ANNEALING.

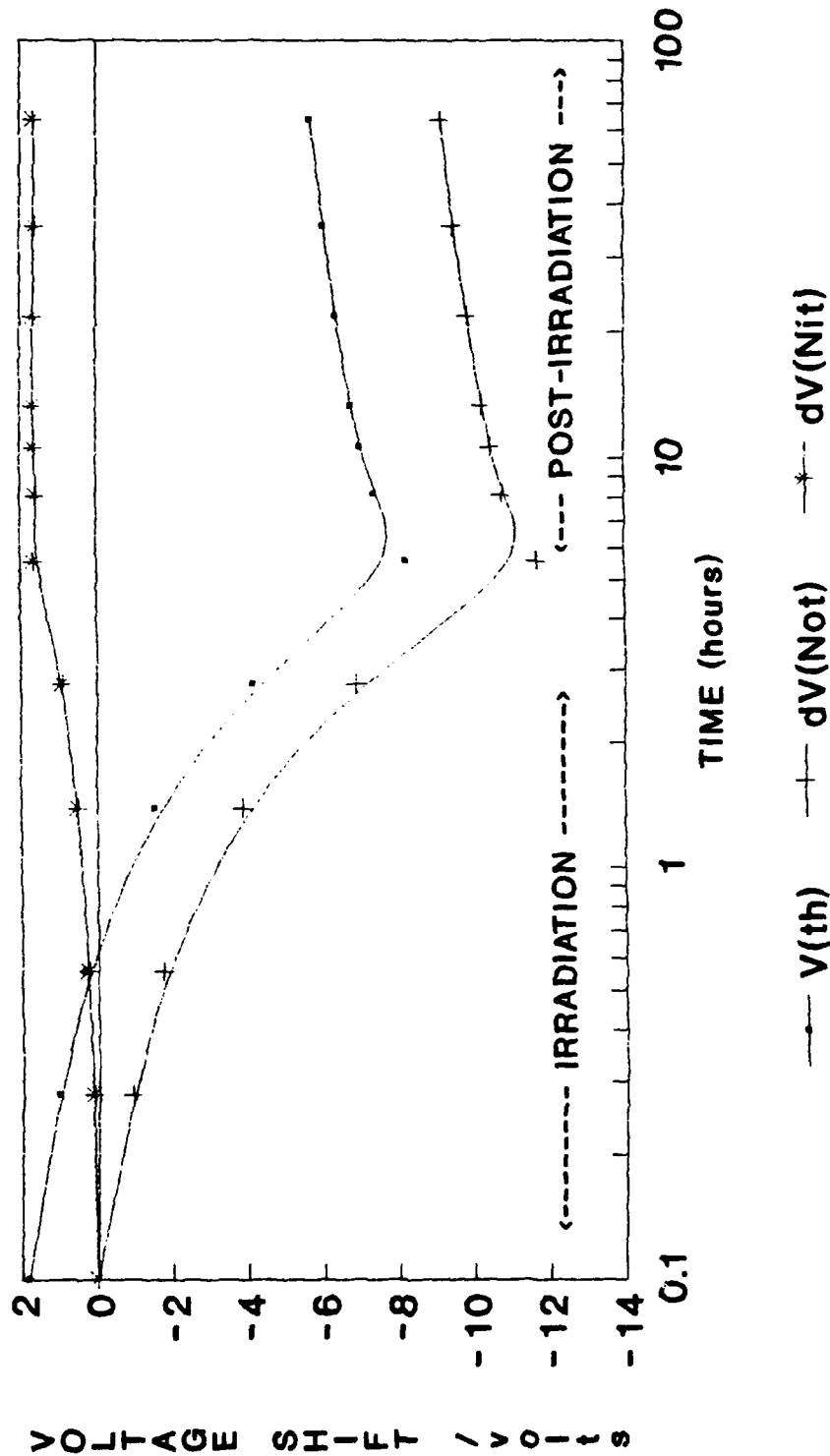


Fig. 9.

3N171 N-CHANNEL MOSFET.  
GATE VOLTAGE-5V. TEMPERATURE-25C.

Figure 9: Plots of  $\Delta V_{th}$ ,  $\Delta V_{ot}$  and  $\Delta V_{it}$  for the 3N171 both during and after steady-state irradiation. The parameters were derived using the techniques described in the text.

# EFFECTS OF TEMPERATURE ON ANNEALING CHARACTERISTICS OF 3N171 MOSFET

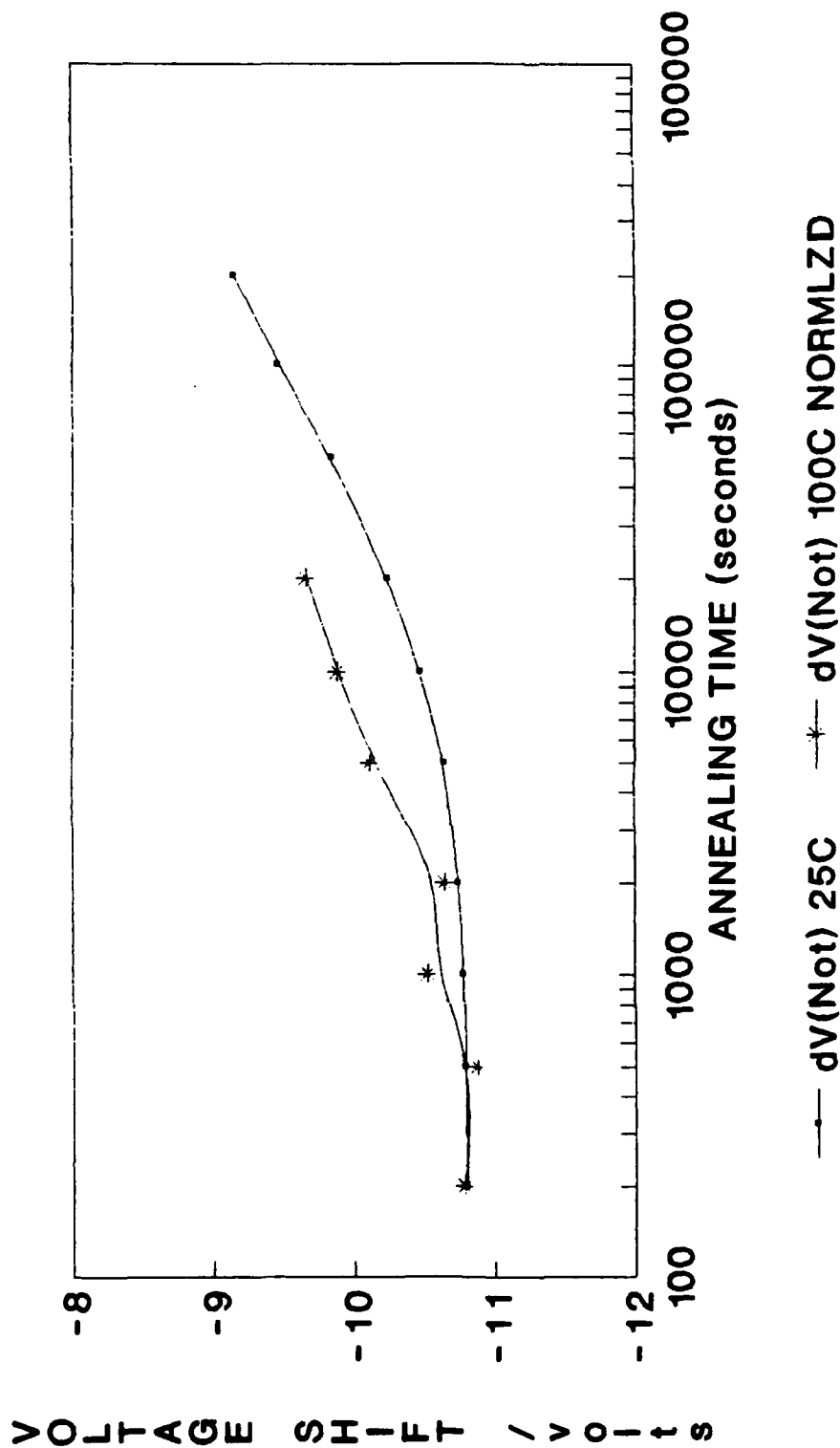


Fig. 10.

3N171 N-CHANNEL MOSFET  
GATE VOLTAGE=5V.

Figure 10: Comparison of the annealing characteristics of  $\Delta V_{or}$  of the 3N171 at  $T = 25^\circ\text{C}$  and  $T = 100^\circ\text{C}$ . The enhanced annealing at the higher temperatures is apparent.

# EFFECTS OF TEMPERATURE ON IN-FLUX CHARACTERISTICS OF 3N171 MOSFET

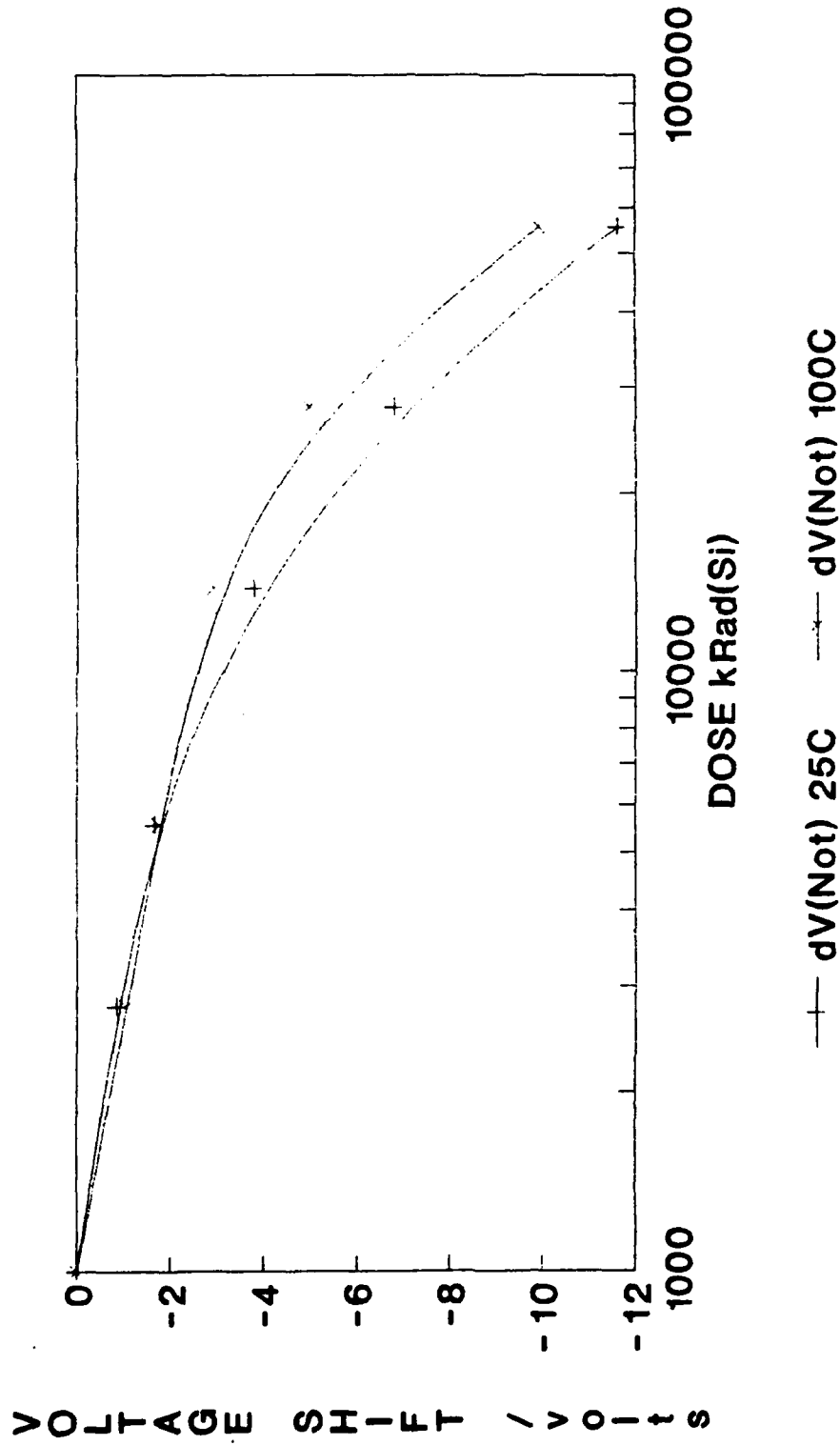


Figure 11: In-flux characteristics of the 3N171 for steady-state irradiations at 25°C and 100°C. Note that more traps are filled at 25°C, due to the higher temperature de-trapping.

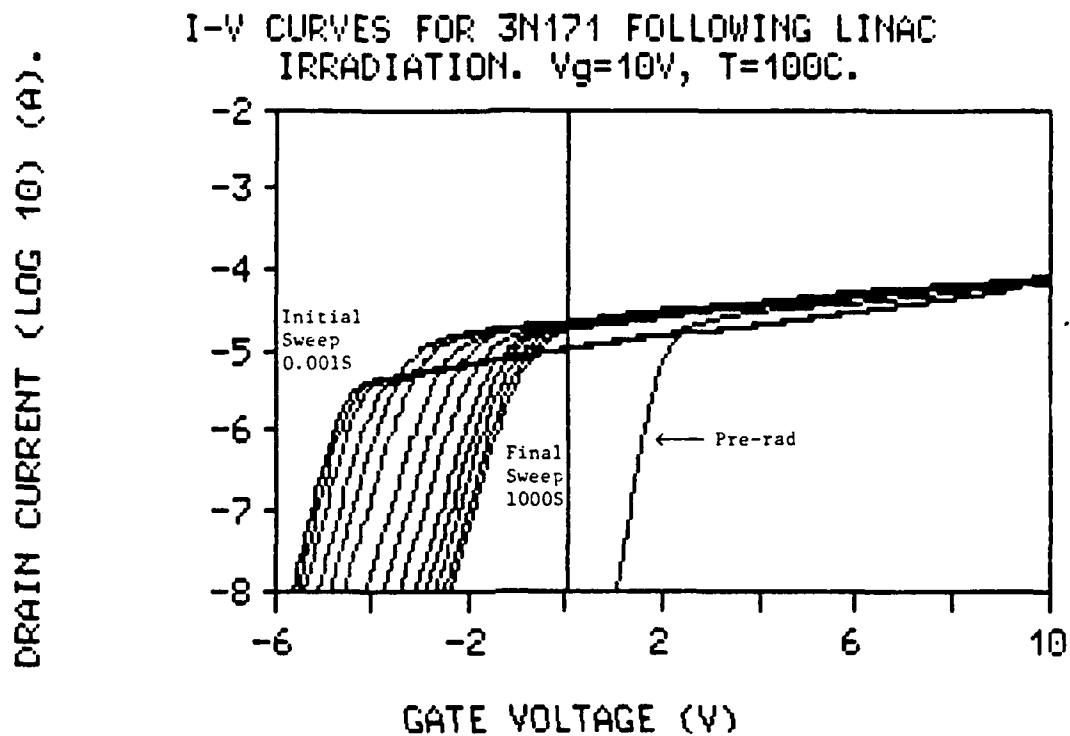


Figure 12: I-V response curves of the 3N171 ( $V_g = 5V$ ,  $T = 100^{\circ}C$ ) following LINAC irradiation.

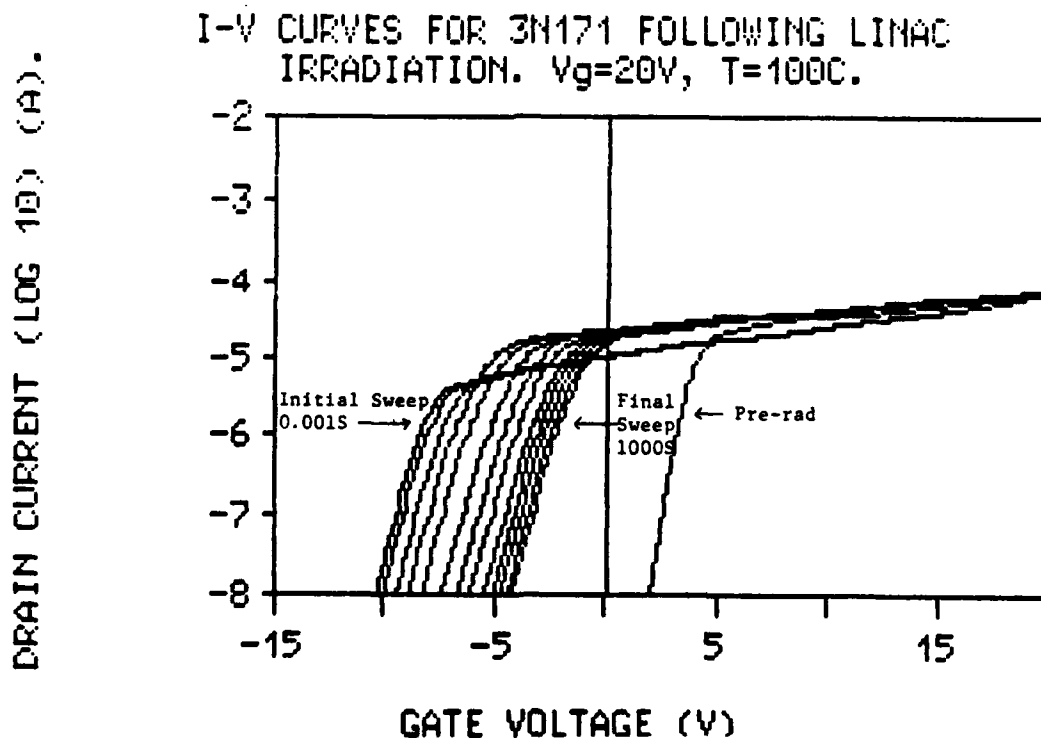
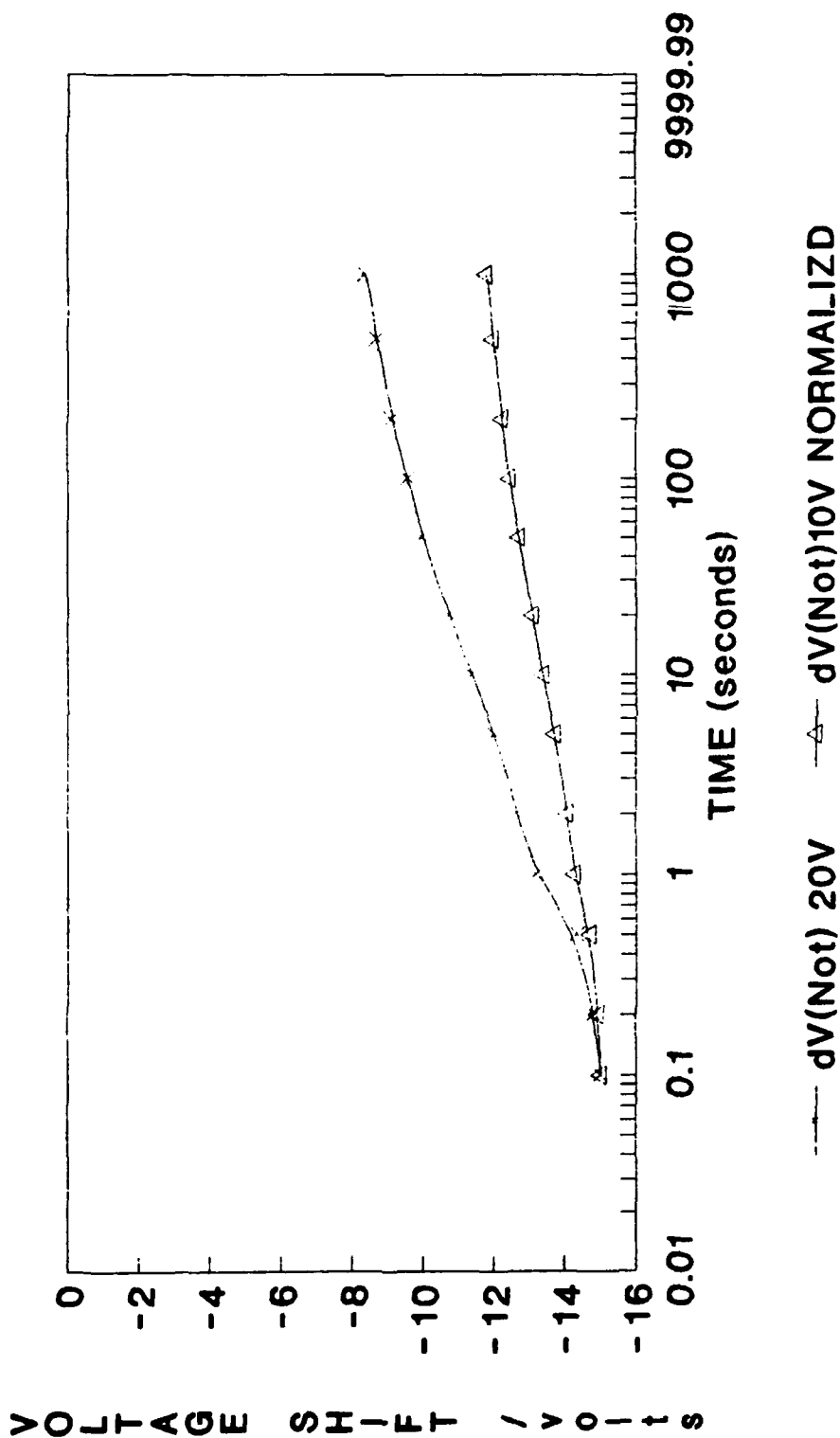


Figure 13: I-V response curves of the 3N171 ( $V_g = 20V$ ,  $T = 100^{\circ}C$ ) following LINAC irradiation.

# ENHANCED ANNEALING EFFECT AT HIGHER GATE VOLTAGE.



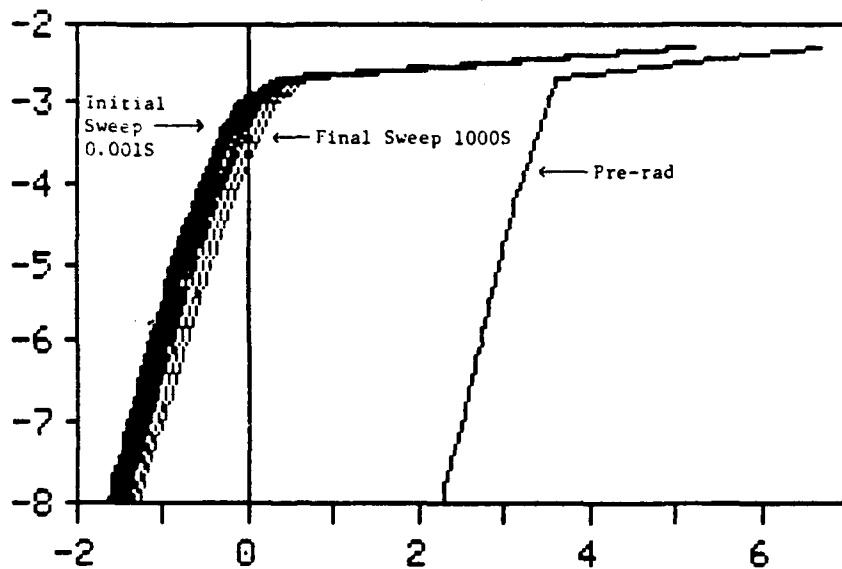
3N171, N-CHAN MOSFET,  $V_g=10V$ ,  $20V$ ,  $T=100$   
SINGLE SHOT LINAC PULSE. DOSE-22.7KRADS

Figure 14: Plot of  $\Delta V_{OT}$  following LINAC irradiation for the two gate biases in fig (12) and fig (13). The accelerated annealing due to higher bias is readily apparent.



DRAIN CURRENT (LOG 10) (A).

I-V CURVES FOR 2N12 FOLLOWING LINAC IRRADIATION.  $V_g=5V$ ,  $T=25^\circ C$ .

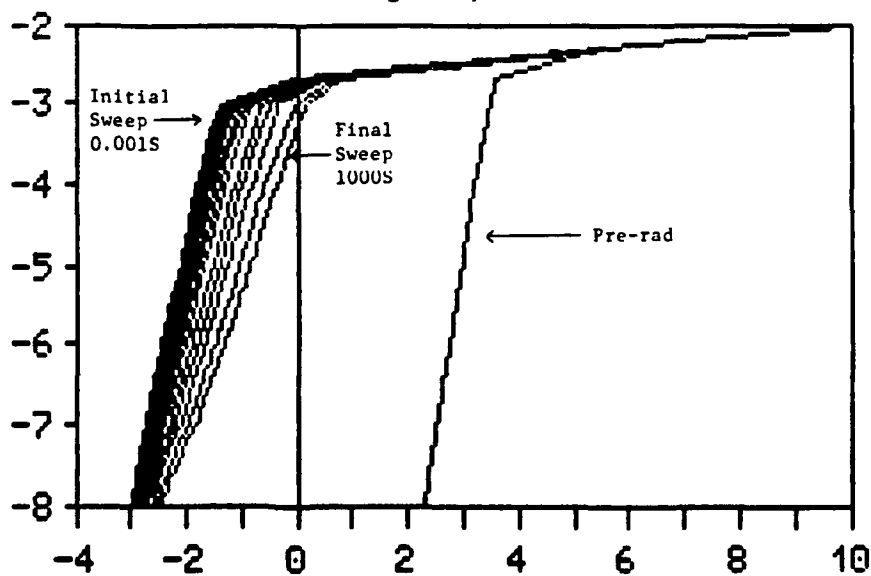


GATE VOLTAGE (V)

Figure 15: I-V response curves of the 2N12 ( $V_g = 5V$ ,  $T = 25^\circ C$ ) to LINAC irradiation.

DRAIN CURRENT (LOG 10) (A).

I-V CURVES FOR 2N12 FOLLOWING LINAC IRRADIATION.  $V_g=5V$ ,  $T=100^\circ C$ .



GATE VOLTAGE (V)

Figure 16: I-V response curves of the 2N12 ( $V_g = 5V$ ,  $T = 100^\circ C$ ) to LINAC irradiation. Compare with Figure 15.

DRAIN CURRENT (LOG 10) (A).

I-V CURVES FOR 2N12 FOLLOWING LINAC IRRADIATION.  $V_g=10V$ ,  $T=25^\circ C$ .

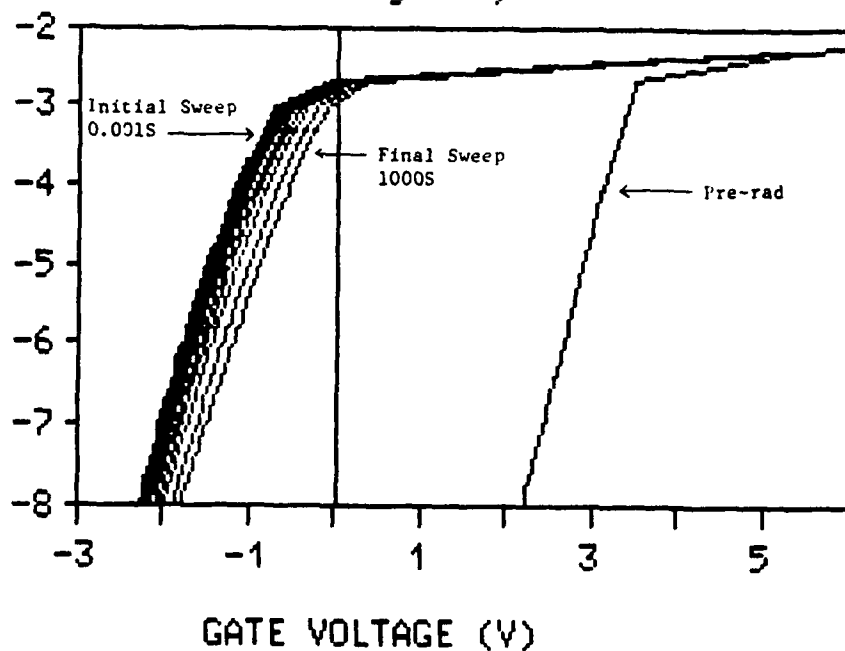


Figure 17: I-V response curves of the 2N12 ( $V_g = 10V$ ,  $T = 25^\circ C$ ) to LINAC irradiation.

DRAIN CURRENT (LOG 10) (A).

I-V CURVES FOR 2N12 FOLLOWING LINAC IRRADIATION.  $V_g=10V$ ,  $T=100^\circ C$ .

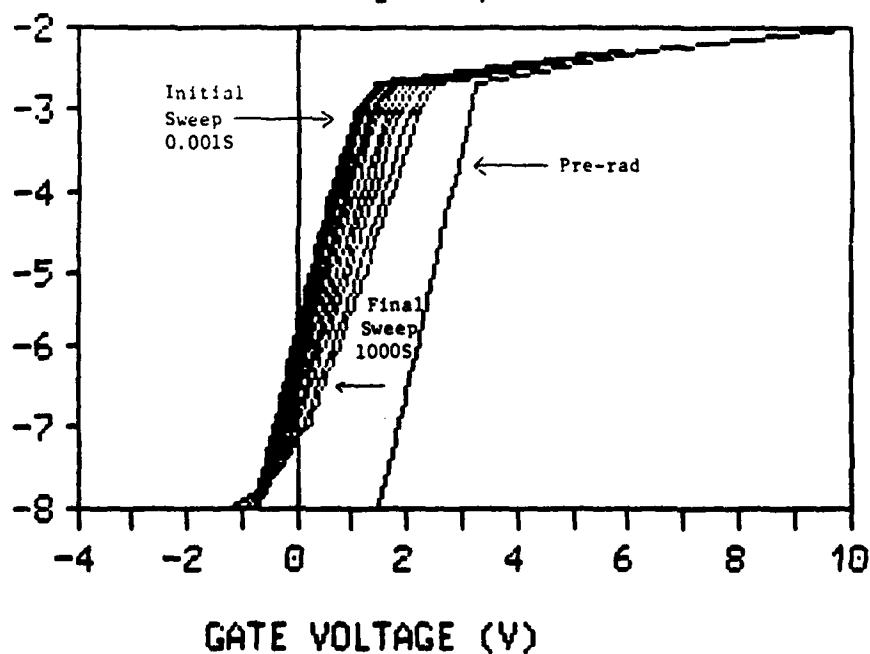
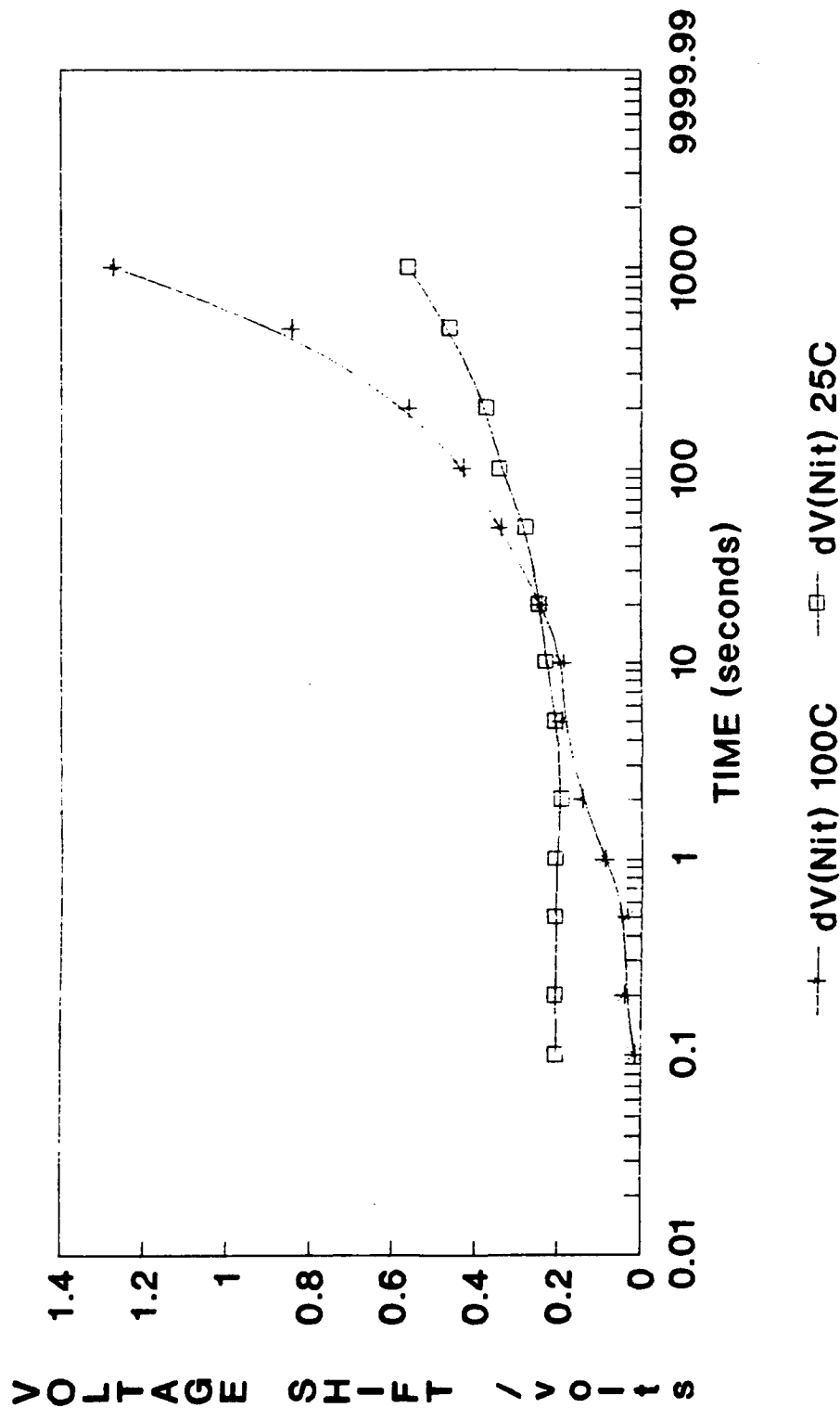


Figure 18: I-V response curves of the 2N12 ( $V_g = 10V$ ,  $T = 100^\circ C$ ) to LINAC irradiation. Compare with Figure 17.

# Vit CHARACTERISTICS FOR 2N12 AT HIGH TEMPERATURE



2N12, N-CHAN MOSFET,  $V_g=10V$ .

Figure 19:  $\Delta V_{it}$  characteristics of the 2N12 ( $V_g = 10V$ ) for two different temperatures following LINAC irradiation. Note the "stretchout" behaviour, and the effect of temperature.

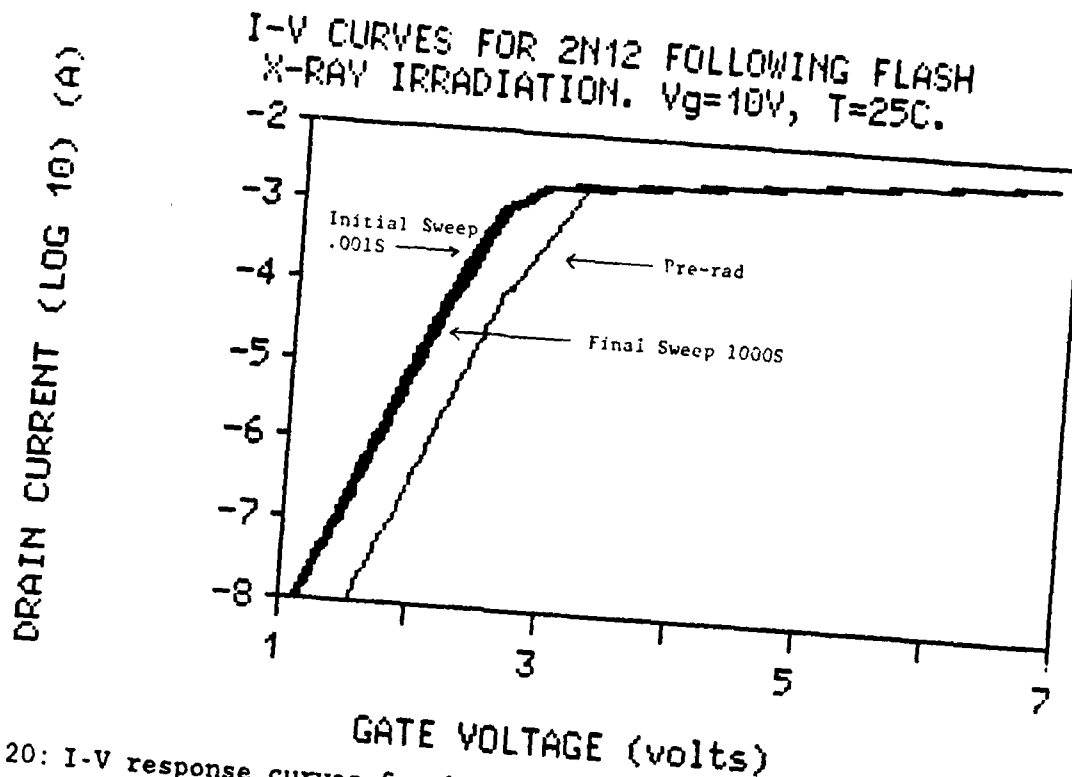


Figure 20: I-V response curves for 2N12 ( $V_g = 10V$ ,  $T = 25^\circ C$ ) following Flash X-ray irradiation. Note the small shift due to smaller total dose, albeit higher dose rate than for the LINAC.

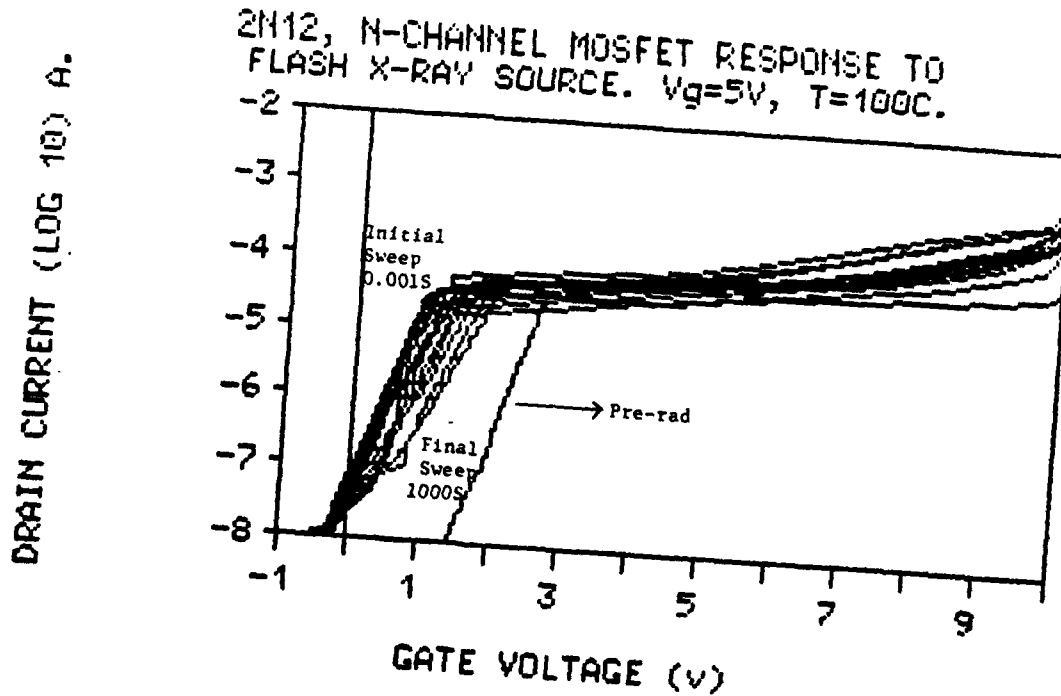


Figure 21: I-V response curves for 2N12 ( $V_g = 5V$ ,  $T = 100^\circ C$ ) following Flash X-ray irradiation. (Total dose  $\approx 10$  kRad(Si)).

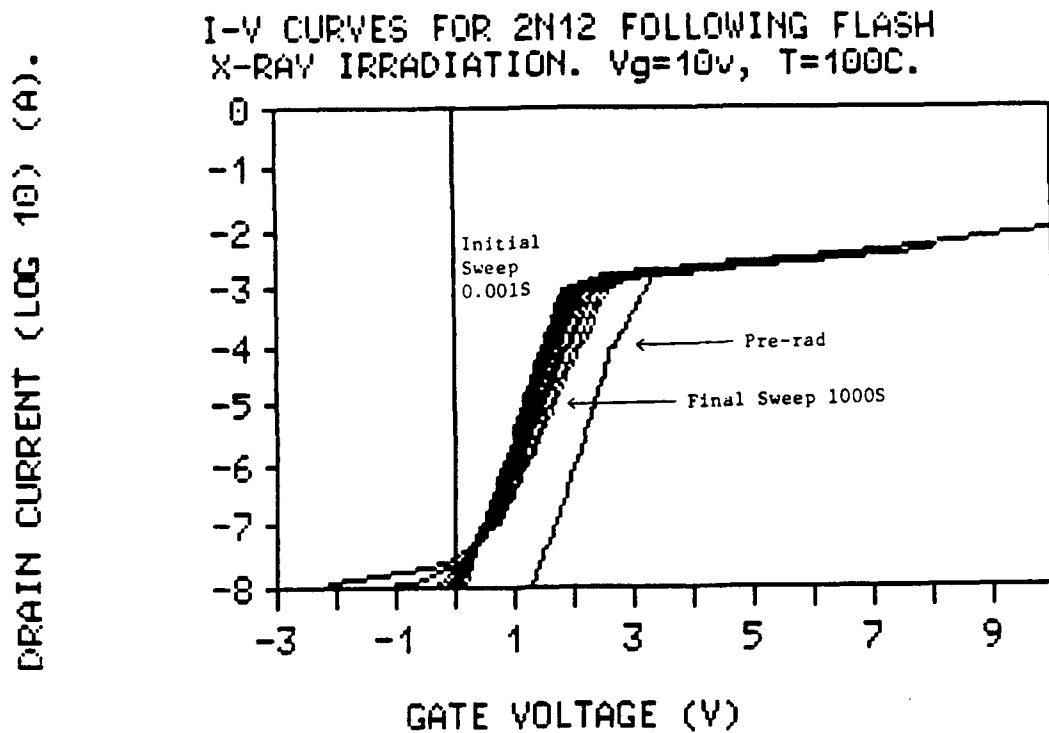


Figure 22: I-V response curves for 2N12 ( $V_g = 10V$ ,  $T = 100^\circ C$ ) following Flash X-ray irradiation. (Total dose  $\approx 10$  kRad(Si)). A comparison with fig 21 shows the effect of higher gate bias on "stretchout".

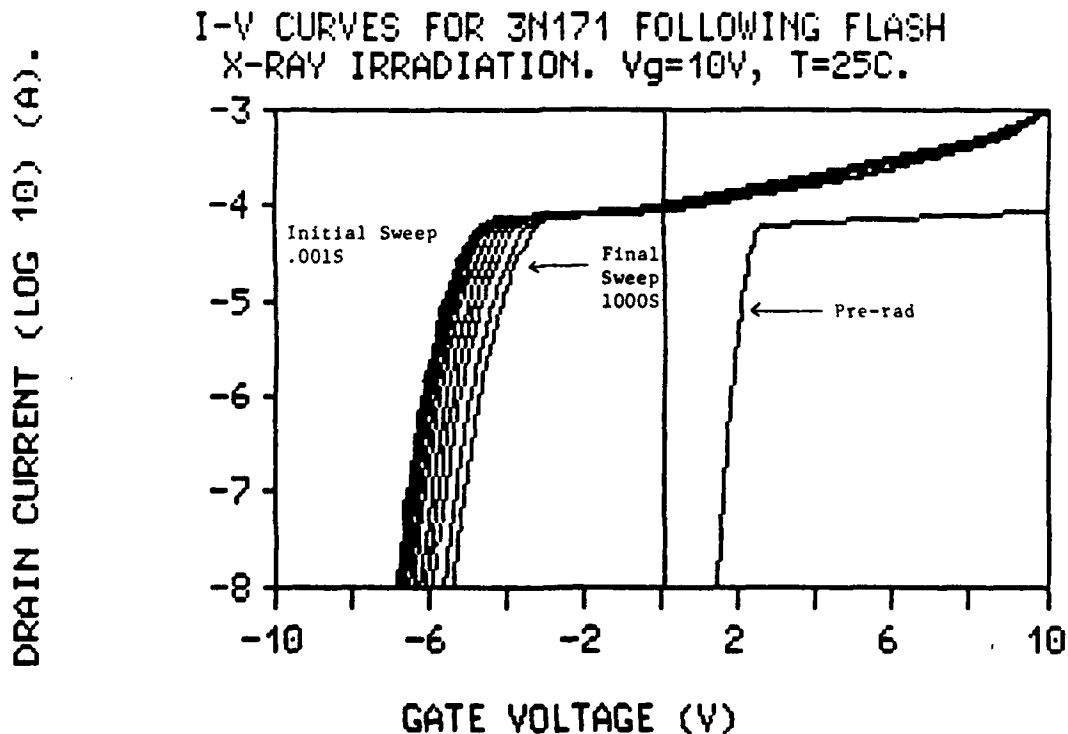


Figure 23: I-V response curves for 3N171 ( $V_g = 10V$ ,  $T = 25^\circ C$ ) following Flash X-ray irradiation. (Total dose  $\approx 10$  kRad).

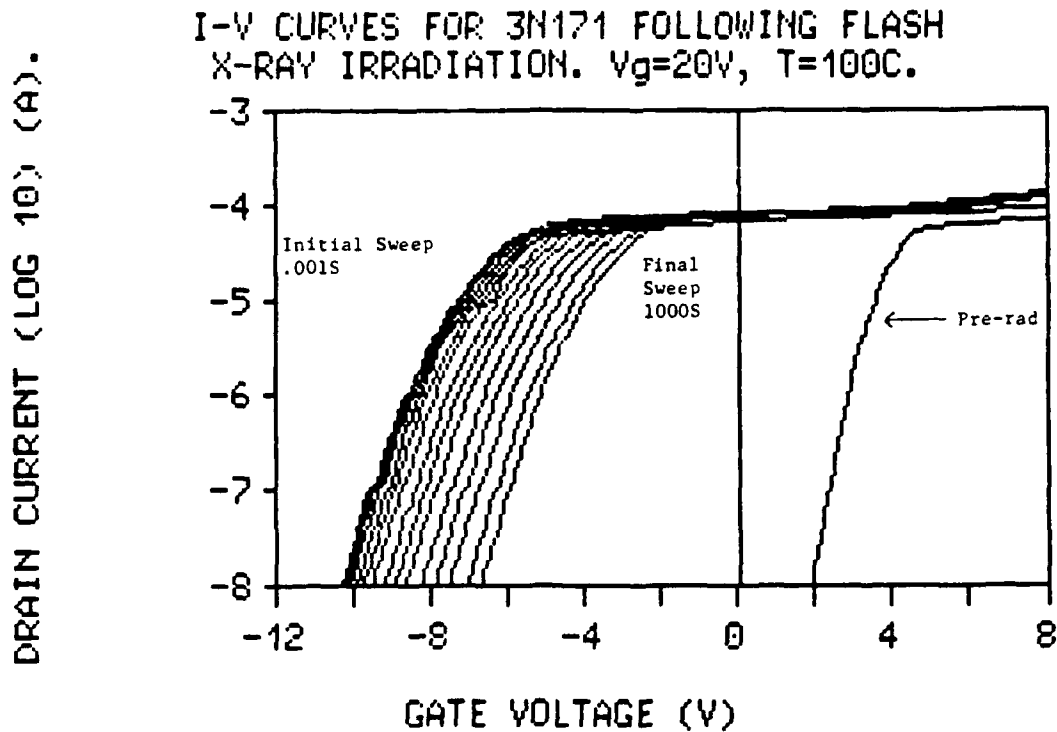


Figure 24: I-V response curve for 3N171 ( $V_g = 20V$ ,  $T = 100^\circ C$ ) following Flash X-ray irradiation. (Total dose  $\approx 10$  kRad). The enhanced annealing compared to that in fig 23 is readily apparent.

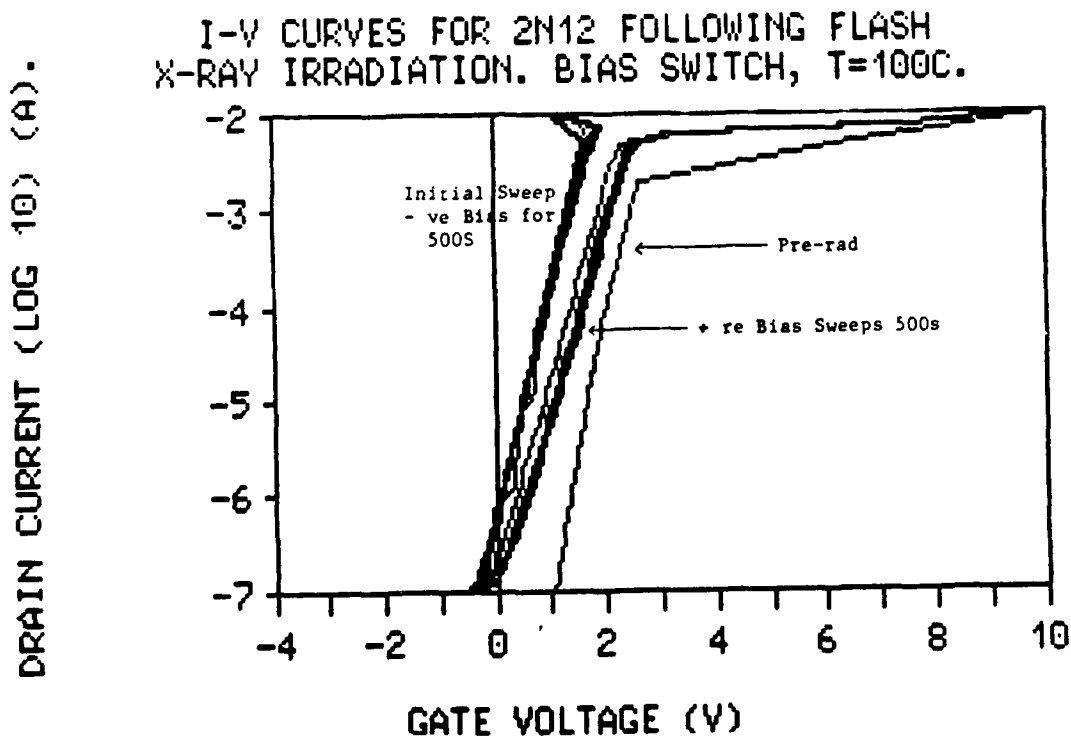
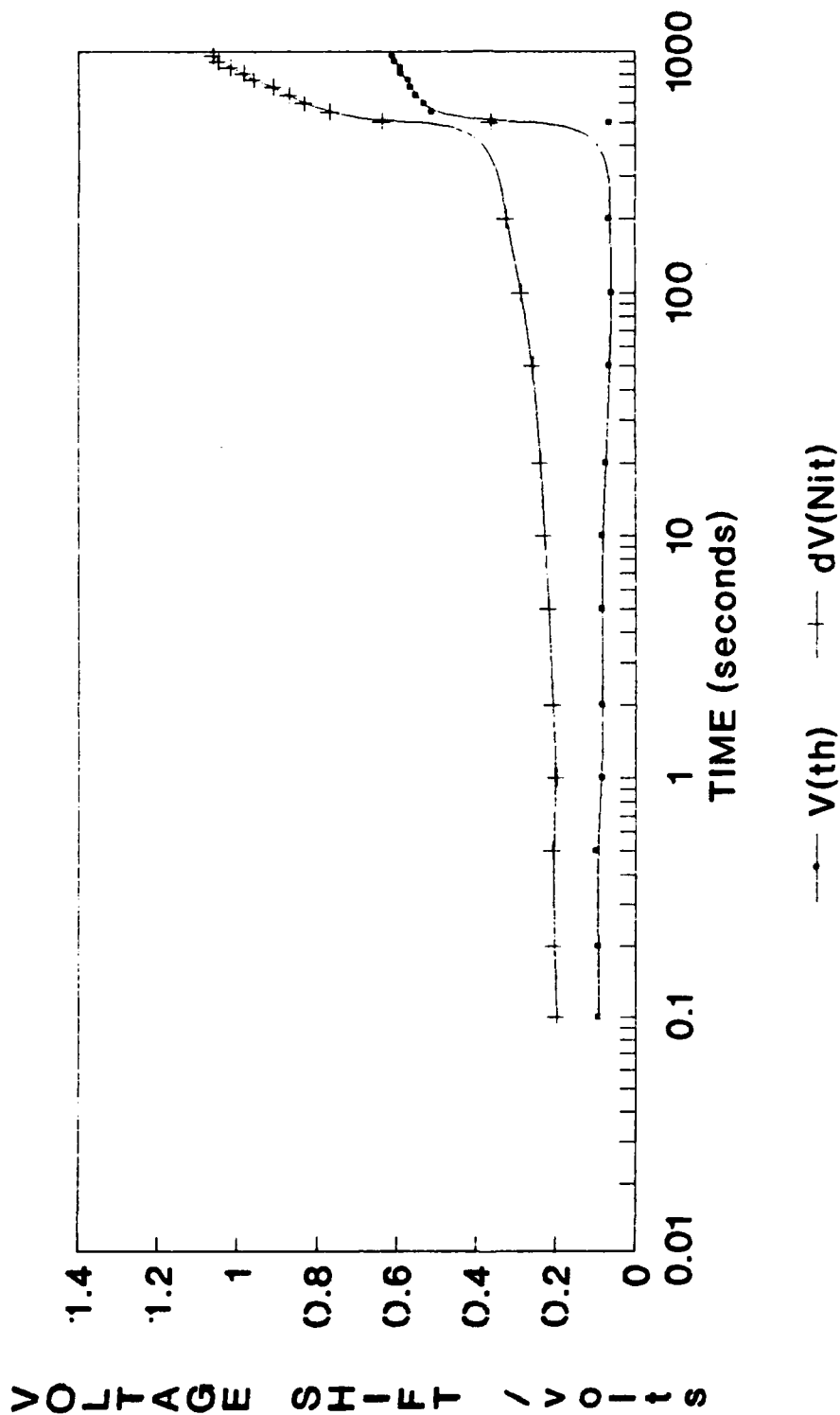


Figure 25: I-V response curves for 2N12 ( $V_g = +10V$ ,  $T = 100^\circ C$ ), with bias switching as described in text, following Flash X-ray irradiation.

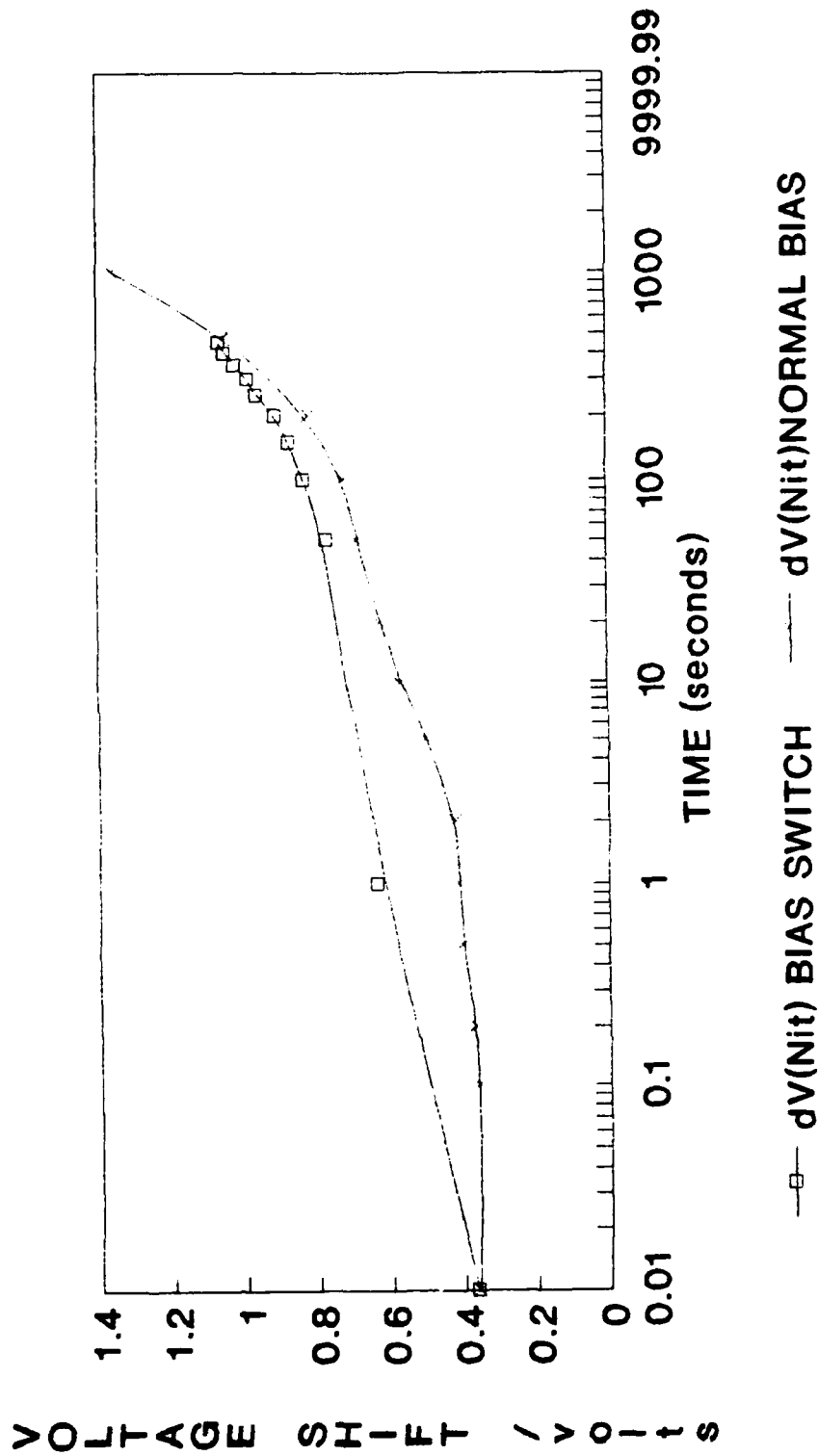
# V<sub>it</sub> BEHAVIOR OF 2N12 FOR SWITCHED BIAS TEST.



2N12 N-CHAN. MOSFET,  $V_g = -5V$  for initial  
500 seconds then switched to +5v. T=100C

Figure 26:  $\Delta V_{IT}$  behaviour of 2N12 for the switched bias test.

# COMPARISON OF ANNEALING CHARACTERISTICS FOR SWITCHED BIAS AND NORMAL CONDITIONS FOR 2N12



switched bias conditions:  $V_g = -5v$  for  
initial 500s then switched to  $+5v$ .

Figure 27: Comparison of annealing characteristics for switched bias and normal ( $+10V$ ) conditions for 2N12.



## 5.0 REFERENCES

1. Tausch H.J., R. Wemhoner, R.L. Pease, J.R. Schwank and R.J. Maier, IEE Trans. Nuc. Sci., NS-34, 6(1987) p1763.
2. McLean F.B. and T.R. Oldham, "Basic Mechanisms of Radiation Effects in Electronic Materials and Devices", Tutorial Short Course, 1987 IEEE Nuclear Space and Radiation Effects Conference, Snowmass, Co.
3. Evans J. "Fundamental Principles of Transistors", Heywood and Co, London, 1957, p196.
4. Ausman G.A. and F.B. McLean, Appl. Phys. Lett., 26 (1975) p173.
5. Montroll E.W. and G.H. Weiss, J. Math. Phys., 6 (1965) p167.
6. Scher H. and M. Lax, Phys. Rev., B7 (1973) p4491.
7. McLean F.B. and G.A. Ausman, Phys. Rev. B., 15 (1977) p.1052.
8. McGowan S. "Evaluation of dual MOSFET gamma-radiation sensors fabricated by Carelton University" DREO Technical Note, DREO-TN-86-4, 1986.
9. Saks N.S., M.G. Ancona and J.A. Modolo, IEEE Trans. Nucl. Sci., NS-31 (1984), p1249.
10. Bendetto J.M., H.E. Boesch, F.B. McLean and J.P. Mize, IEEE Trans. Nucl. Sci., NS-32 (1985) p3916.
11. Manzini S. and A. Modelli, "Insulating Films on Semiconductors", North-Holland, New York, 1983, p112.
12. Oldham T.R., A.J. Lelis and F.B. McLean, IEEE Trans. Nucl. Sci. NS-33 (1986) p1203.
13. Cousins T., "Pulse-Width Dependent Radiation Effects on Electronic Components" DREO Technical Note, To Be Published.
14. McLean F.B., IEEE Trans. Nucl. Sci., NS-35, (1988) p1178.
15. Sze, S.M. "Physics of Semiconductor Devices" 2nd Ed., John Wiley and Sons, New York, 1981, p446.
16. McWhorter P.J. and P.S. Winokur, Appl. Phys. Lett., 48(2) (1986) p133.
17. Winokur P.J., private communication.

18. Boesch, H.E., IEEE Trans. Nucl. Sci., NS-33 (1986) p1337.
19. Cousins, T. "Canadian TREE facilities", presented at US/CA MDEA meeting, Ottawa, Aug. 1989.
20. Kazi, A.H., T. Cousins and D.M. Eagleson "1986 NATO Battlefield Dosimeter Intercomparison Data Summary", USA CSTA Report No. 6478, 4 Feb 1987.
21. Lelis A.J., H.E. Boesch, T.R. Oldham and F.B. McLean, IEEE Trans. on Nucl. Sci., NS-35 (1988) p1382.

SECURITY CLASSIFICATION OF FORM  
(highest classification of Title, Abstract, Keywords)

**DOCUMENT CONTROL DATA**

(Security classification of title, body of abstract and indexing annotation must be entered when the overall document is classified)

1. ORIGINATOR (the name and address of the organization preparing the document. Organizations for whom the document was prepared, e.g. Establishment sponsoring a contractor's report, or tasking agency, are entered in section 8.)  Defence Research Establishment Ottawa Ottawa, Ontario K1A 0Z4		2. SECURITY CLASSIFICATION (overall security classification of the document including special warning terms if applicable)  UNCLASSIFIED	
3. TITLE (the complete document title as indicated on the title page. Its classification should be indicated by the appropriate abbreviation (S,C,R or U) in parentheses after the title.)  Transient Annealing Characterization of Irradiated MOSFETS (U)			
4. AUTHORS (Last name, first name, middle initial)  Cousins, T. and Qureshi, K.M.			
5. DATE OF PUBLICATION (month and year of publication of document)		6a. NO. OF PAGES (total containing information. Include Annexes, Appendices, etc.) 43	6b. NO. OF REFS (total cited in document) 21
7. DESCRIPTIVE NOTES (the category of the document, e.g. technical report, technical note or memorandum. If appropriate, enter the type of report, e.g. interim, progress, summary, annual or final. Give the inclusive dates when a specific reporting period is covered.)  Technical Report			
8. SPONSORING ACTIVITY (the name of the department project office or laboratory sponsoring the research and development. Include the address.) Defence Research Establishment Ottawa Ottawa, Ontario K1A 0Z4			
9a. PROJECT OR GRANT NO. (if appropriate, the applicable research and development project or grant number under which the document was written. Please specify whether project or grant)  Project No. 041LS		9b. CONTRACT NO. (if appropriate, the applicable number under which the document was written)	
10a. ORIGINATOR'S DOCUMENT NUMBER (the official document number by which the document is identified by the originating activity. This number must be unique to this document)  DREO REPORT 1030		10b. OTHER DOCUMENT NOS. (Any other numbers which may be assigned this document either by the originator or by the sponsor)	
11. DOCUMENT AVAILABILITY (any limitations on further dissemination of the document, other than those imposed by security classification) (X) Unlimited distribution ( ) Distribution limited to defence departments and defence contractors; further distribution only as approved ( ) Distribution limited to defence departments and Canadian defence contractors; further distribution only as approved ( ) Distribution limited to government departments and agencies; further distribution only as approved ( ) Distribution limited to defence departments; further distribution only as approved ( ) Other (please specify):			
12. DOCUMENT ANNOUNCEMENT (any limitation to the bibliographic announcement of this document. This will normally correspond to the Document Availability (11). However, where further distribution (beyond the audience specified in 11) is possible, a wider announcement audience may be selected.)			

13. ABSTRACT (a brief and factual summary of the document. It may also appear elsewhere in the body of the document itself. It is highly desirable that the abstract of classified documents be unclassified. Each paragraph of the abstract shall begin with an indication of the security classification of the information in the paragraph (unless the document itself is unclassified) represented as (S), (C), (R), or (U). It is not necessary to include here abstracts in both official languages unless the text is bilingual).

The electrical response of metal-oxide-silicon (MOS) technologies to incident nuclear (especially photon) radiation is a very complex, time-dependent function. This report reviews the physical processes governing this response and then experimentally examines them with the aid of the TATS-400 (Transient Annealing Test System). MOSFET responses to steady-state and pulsed photon and electron beams are characterized in terms of such parameters as threshold voltage shift and interface and oxide trap densities. The results show good agreement between experiment and theory in terms of the expected trends, however in order to conduct more meaningful tests, devices with much better-known geometries must be procured.

14. KEYWORDS, DESCRIPTORS or IDENTIFIERS (technically meaningful terms or short phrases that characterize a document and could be helpful in cataloguing the document. They should be selected so that no security classification is required. Identifiers, such as equipment model designation, trade name, military project code name, geographic location may also be included. If possible keywords should be selected from a published thesaurus. e.g. Thesaurus of Engineering and Scientific Terms (TEST) and that thesaurus-identified. If it is not possible to select indexing terms which are Unclassified, the classification of each should be indicated as with the title.)

Transient Radiation Effects on Electronics,  
Metal-Oxide-Silicon Field Effect Transistor,  
Nuclear Radiation  
Gamma Rays,  
Electrons/Holes,  
Dose.  
Dose Rate,  
Annealing.

Source (R14)  
A